The chronostratigraphy of the Haua Fteah cave (Cyrenaica, northeast Libya) — optical dating of early human occupation during Marine Isotope Stages 4, 5 and 6

Zenobia Jacobs[a*], Bo Li[a], Lucy Farr[b], Evan Hill[c], Chris Hunt[d], Sacha Jones[b], Ryan Rabett[c], Tim Reynolds[e], Richard G. Roberts[a], David Simpson[c], Graeme Barker[b]

[a] ARC Centre of Excellence for Australian Biodiversity and Heritage & Centre for Archaeological Science, School of Earth and Environmental Sciences, University of Wollongong, New South Wales 2522, Australia

[b] McDonald Institute for Archaeological Research, University of Cambridge, Cambridge CB2 3ER, UK

[c] School of Geography, Archaeology and Palaeoecology, Queens University Belfast, Belfast BT7 1NN, UK

[d] School of Natural Sciences and Psychology, Liverpool John Moores University, Liverpool L3 3LH, UK

[e] Department of History, Classics and Archaeology, Birkbeck College, University of London, London WC1B 5DQ, UK

* Corresponding author: zenobia@uow.edu.au

Abstract

The paper presents the results of optical dating of potassium-rich feldspar grains obtained from the Haua Fteah cave in Cyrenaica, northeast Libya, focussing on the chronology of the Deep Sounding excavated by Charles McBurney in the 1950s and re-excavated recently. Samples were also collected from a 1.25 m-deep trench (Trench S) excavated during the present project below the basal level of the Deep Sounding. Optically stimulated luminescence (OSL) data sets for multi-grain, single aliquots of quartz for samples from the Middle Trench were previously published. Re-analyses of these OSL data confirm significant variation in the dose saturation levels of the quartz signal, but allow the most robust OSL ages to be determined for comparison with previous age estimates and with those obtained in this study for potassium-rich feldspars from the Deep Sounding. The latter indicate that humans may have started to visit the cave as early as ~150 ka ago, but that major use of the cave occurred during MIS 5, with the accumulation of the Deep Sounding sediments. Correlations between optical ages and episodes of "Pre-Aurignacian" artefact discard indicate that human use of the cave during MIS 5 was highly intermittent. The earliest phases of human activity appear to have occurred during interstadial conditions (5e and 5c), with a later phase of lithic discard associated with more stadial conditions, possibly MIS 5b. We argue that the "Pre-Aurignacian" assemblage can probably be linked with modern humans, like the succeeding "Levalloiso-Mousterian" assemblage; two modern human mandibles associated with the latter are associated with a modelled age of 73–65 ka. If this attribution is correct, then the new chronology implies that modern humans using "Pre-Aurignacian" technologies were in Cyrenaica as early as modern humans equipped with "Aterian" technologies were in the Maghreb, raising new questions about variability among lithic technologies during the initial phases of modern human dispersals into North Africa.

Keywords: OSL; MET-pIRIR; Middle Stone Age; North Africa; modern humans

Introduction

The Haua Fteah, located at 22°3'5"E and 32°53'70"N, is a large limestone phreatic cave remnant at the foot of the northern escarpment of the Gebel Akhdar ('Green Mountain') massif, overlooking the present-day coast of Cyrenaica, northeast Libya (Fig. 1a). The north-facing entrance (Fig. 1b) is ~1 km from the coast and is ~50 m wide and ~20 m high; the interior roofed area measures ~80 m across. Excavations by Charles McBurney over three seasons (1951, 1952 and 1955: Fig. 1c) revealed a 14 m-deep sequence of cultural deposits, which has since been used as a key reference sequence for North Africa. At the completion of McBurney's excavations, the trench consisted of three stepped units (Fig. 1d): an Upper Trench (our terminology, not McBurney's) measuring approximately 10 × 11 m surface area x 2 m deep; a Middle Trench measuring about 7 × 6 × 5.5 m; and a Deep Sounding that was published by McBurney (1967) as being 2.5 × 1.5 × 6.5 m, although we measured it in 2012 as 3.8 × 1.6 × 6.5 m. It is known that the Deep Sounding was expanded rapidly at the end of the 1955 season and was not fully recorded by McBurney. Most of his excavation, the deeper layers especially, was undertaken using horizontal spits, so his samples of lithics and fauna can cross-cut different sedimentary units. He used the (then recent) technique of radiocarbon (^{14}C) dating to establish a numerical chronology for the uppermost 7 m of the sequence and, from these ages, estimated the sedimentation rate to infer an age of ~80 ka for the base of the deposit, marked by rockfall at the base of the Deep Sounding.

McBurney (1967) defined seven cultural phases of occupation, based on the typology and technology of the lithic material recovered. The earliest phase (A), from spit 176 (at the bottom of the Deep Sounding) to spit 50 (underlying Layer XXXV at the base of the Middle Trench), was a Middle Stone Age (MSA) industry based on flakes and blades which he termed the "Pre-Aurignacian" because it was taken to resemble the Pre-Aurignacian and Amudian assemblages in Southwest Asia. This was overlain (Phase B: Layers XXXV–XXV) by "Levalloiso-Mousterian" industries, so called from their broad comparability with these industries in the Levant and Europe. Two human mandibles in Layer XXXIII were originally regarded as 'Neanderthaloid', but have since been confirmed as an early form of modern human (Hublin, 2000). Phase C (upper part of Layer XXV to Layer XVI) was an industry characterized by blade technology and an Upper Palaeolithic tool inventory.

McBurney termed this the “Dabban” after the Cyrenaican cave of Hagfet ed-Dabba where he had found similar material (McBurney, 1960). The Dabban was succeeded by a microlithic late or final Upper Palaeolithic industry (Phase D, Layers XV–XI) and termed the “Eastern Oranian” or Iberomaurusian from its similarities with assemblages in the Maghreb (northwest Africa). At the junction of the Middle and Upper Trenches (Phase E, Layers X and IX) was a microlithic Mesolithic-type industry with parallels to Capsian assemblages in the Maghreb and, hence, classified as the “Libyco-Capsian”. Above this was the final prehistoric occupation (Phase F, Layers VIII–IV), with Neolithic pottery and domestic sheep and goats, which was termed “Neolithic of Libyco-Capsian tradition” because of similarities in stone tools (the frequency of backed pieces, for example) with the preceding Libyco-Capsian. The prehistoric sequence was capped (Phase G) by a substantial boulder-supported structure dating to the Graeco-Roman period (Layers III and II), covered by burnt animal dung and other evidence of animal enclosures, dating to recent centuries (Layer I). The cave is still used for stalling sheep and goats, and similar deposits continue to accumulate.

McBurney’s excavations were remarkable in their scale, especially given the considerable logistical problems faced by his team, and the subsequent analyses of the material were pioneering for their time (McBurney, 1967). However, techniques of cave stratigraphic analysis, excavation, numerical dating and archaeological science more generally have all been transformed in the subsequent half century, providing the context for the renewal of fieldwork in 2007 (Barker et al., 2007, 2008, 2009, 2010, 2012; Rabett et al., 2013; Farr et al., 2014; and see Acknowledgements). In the course of eight seasons of fieldwork (the last completed by the Libyan members of the team in 2015, when security conditions prevented further fieldwork by the international team), we have removed the backfill deposited in the McBurney trench at the end of the 1955 season and cleaned and recorded the original sections using the UK single-context system (Fig. 2). We have excavated new trenches (Fig. 1d) on the southern side of the Middle Trench (Trench M) and the Deep Sounding (Trench D), and the base of the Deep Sounding has been extended downwards by 1.25 m (Trench S) to determine whether earlier cultural material is present. These stratigraphic excavations have been linked to extensive studies of artefactual, bioarchaeological and geoarchaeological data to address the integrity of the McBurney cultural phases and the nature of the transitions between them; the activities carried out in

and from the cave; and the palaeoenvironments in which these activities and site formation processes took place.

Douka et al. (2014) reported on the chronostratigraphy of the upper 7.5 m of the Haua Fteah (the Middle and Upper Trenches) using ^{14}C dating of charcoal, land snails and marine shell, optical dating of quartz grains, electron spin resonance dating of tooth enamel, and tephrochronology. A Bayesian statistical model was constructed on the basis of these ages to establish a robust timeframe for this part of the stratigraphy. Five major lithological units or facies were defined by the new work (Inglis, 2012; Fig. 3), with indications that Facies 5 (red-orange silt layers) continued downwards into the Deep Sounding. The exposed part of this facies, at the base of the Middle Trench, was dated to c. 75–65 ka, broadly correlating with Marine Isotope Stage (MIS) 4, which is dated globally to 74–59 ka (Sanchez-Goñi and Harrisson, 2010) or 71–57 ka (Lisiecki and Raymo, 2005). The two modern human mandibles were found within these sediments. Facies 4 (c. 68–47 ka) formed during a period of significant cooling, Facies 3 (c. 47–35 ka) has indications of periods of increasing landscape destabilisation and cold, and Facies 2 (c. 35–12 ka) consists predominantly of éboulis, so the overall sequence correlates broadly with global trends to increasing aridity and decreasing temperature represented by MIS 4, MIS 3 (c. 60–24 ka) and MIS 2 (c. 24–11.7 ka). The sediments in the Deep Sounding, and the Pre-Aurignacian occupation materials within them, were not dated by Douka et al. (2014) because they were still being excavated. This paper now reports on the results of the optical dating program applied to the sediments from the Deep Sounding, and their implications for North African prehistory.

Material and methods

The Deep Sounding and Trench S sediments

McBurney published only the west-facing section of his Deep Sounding and divided it into 21 stratigraphic units, although he mentioned “many more units” in the accompanying text (McBurney, 1967: 11). The survival of many of his aluminium labels in situ allowed direct comparison between the 1955 spits and the ~90 stratigraphic units recognized in the present study (Fig. 4). The densest concentration of the “Pre-Aurignacian” cultural remains that McBurney excavated extends over ~1.2 m depth of sediment, represented by spits 69–176. The highest frequencies of lithic artefacts were recovered from spits 170–174, located

about 3.1–3.9 m below the top of the Deep Sounding. These five spits (170–174) correspond to several of the present project's contexts in the south-facing section (820, 822, 823, 824, 828, 825 and 827, in depositional order from youngest to oldest).

The sediments of the Deep Sounding consist primarily of red-coloured clayey silts, broken intermittently by more yellowish bands and incipient flowstones. Field observations, mollusc analyses and bulk sediment analyses indicate that the sediments accumulated mainly as mass movements of soil associated with fluvial episodes or as in situ sedimentation in standing water; the latter presumably made this part of the cave unattractive for human occupation. Trench S, excavated at the base of the Deep Sounding, exposed a further 1.25 m of red clayey silts interspersed with thin (typically 20–30 mm thick) sheets of more clay-rich sediment. These overlay a jumble of sharp-edged boulders (about 50–80 cm thick), indicating a significant episode of roof collapse (Fig. 5). We ceased excavation at this stage, so the boulders were not removed, but the fact that the silts slope slightly up against the boulders, rather than plunging beneath them, suggests that the rocks were buried by the silts. The latter contained occasional fragments of chert, animal bones and teeth, shell fragments, charcoal and small quantities of often highly fragmented lithic debitage (Rabett et al., 2013), indicating some form of human presence at the site during the accumulation of the Trench S deposits.

There is evidence for bioturbation of the Deep Sounding sediments. Wasp burrows ~8 mm in diameter are common and are likely to be (pene)contemporary with the deposition of the sediments. Animal burrows measuring ~8 cm in diameter can also be seen at a number of locations in the walls of the Deep Sounding, and excavation of Trench D exposed several burrows cutting through the sediments both vertically and horizontally (Fig. 6). It is likely that these burrows were made by mole rats when the Deep Sounding was open in the 1950s, and again in recent years (a recently deceased mole rat was found at the bottom of the Middle Trench, before the Deep Sounding was emptied in 2012). Given the absence of burrows in the parts of the Haua Fteah stratigraphy composed of compact sediments, mole rats appear to have preferentially burrowed in the softer silts. The effects of bioturbation have not altered the overall stratigraphic integrity of the Deep Sounding and Trench S sediments. Both the pollen and molluscan assemblages in the upper part of the Deep Sounding are well-stratified and show abrupt changes between layers, as is the

molluscan assemblage in the lower section of the Deep Sounding and in Trench S (where pollen is badly preserved).

Optical dating

Optical dating provides a means of determining burial ages for sediments (Huntley et al., 1985; Aitken, 1998; Jacobs and Roberts, 2007; Wintle, 2014; Roberts et al., 2015). The method is based on the steady increase in the number of trapped electrons in mineral grains, such as quartz and potassium-rich feldspar (K-feldspar), over time after burial, in response to the energy supplied to the grains by background levels of ionizing radiation from environmental sources. The time elapsed since sediments were last exposed to sufficient heat or sunlight to empty the relevant electron traps can be estimated from measurements of the optically stimulated luminescence (OSL) or infrared stimulated luminescence (IRSL) signals to obtain an estimate of the equivalent dose (D_e), together with determinations of the radioactivity of the sample and the material surrounding it to a distance of ~40 cm to obtain an estimate of the dose rate (D_r). The D_e represents the radiation dose to which sedimentary grains have been exposed in their burial environment, and the D_r represents the rate of exposure of these grains to ionizing radiation over the entire period of burial. The latter is mostly derived from the radioactive decay of ^{238}U, ^{235}U, ^{232}Th (and their daughter products) and ^{40}K external to the dated grains, radioactive inclusions internal to the minerals (^{40}K and ^{87}Rb making a significant contribution to the D_r of sand-sized K-feldspar grains), and a lesser contribution from cosmic rays. The burial age of grains that were well-bleached at the time of deposition can then be calculated by dividing the estimated D_e by the estimate of D_r for the entire period of burial.

Previous studies

We have previously published single grain and multi-grain single aliquot OSL ages for sedimentary quartz from 12 samples collected from the Middle Trench (Douka et al., 2014). The ages for these samples ranged from ~18 to ~72 ka and had D_e values that ranged between ~25 and 130 Gy. The OSL ages for the 12 samples were in correct stratigraphic order for both the small multi-grain aliquots (except sample HF6) and the single grains, and both aliquots and grains produced statistically consistent ages where comparisons were

available. There was generally good correspondence between the OSL ages, ^{14}C ages and the ages of the tephra horizons, apart from an apparent mismatch between the OSL age for HF8 of 46 ± 5 ka and the age 68.6 ± 2.1 ka for the tephra (T513) found in the same context (see Douka et al., 2014, for explanation of this and for discussion of the two OSL ages published by Russell and Armitage, 2012). None of the OSL samples was directly comparable stratigraphically with the Campanian Ignimbrite (CI) tephra (T441/442), but two of the OSL samples (HF4 and HF5) bracket this layer. Sample HF5, located ~30 cm below T441/442 and dated to 47 ± 5 ka, is older than the CI tephra, and sample HF4, located ~20 cm above T441/442, yielded an age of 38 ± 4 ka, which corresponds closely with the $^{40}Ar/^{39}Ar$ age of 39.28 ± 0.11 ka for the CI tephra (De Vivo et al., 2001). The uppermost and macroscopically visible tephra layer (T426) is located immediately beneath OSL sample HF2, which gave an age of 18 ± 1 ka. This is statistically consistent with the age of 16.8–17.9 ka cal BP (95% confidence interval) assigned to the tephra and with a range of ^{14}C ages. These independent checks on the OSL chronology gave us confidence in the ages for at least the upper half of the Middle Trench.

The lowest samples (HF10, HF11 and HF12) near the base of the Middle Trench, however, had dose response curves for many of the grains and aliquots that were close to saturation (see Fig. 6 in Douka et al., 2014). It is well-known that D_e estimation in the high dose range of OSL quartz is problematic and can result in underestimation of the true burial age; in such cases, only minimum ages for the samples can be obtained (e.g., Lowick and Preusser, 2011; Chapot et al., 2012; Duller et al., 2015).

To further investigate issues of saturation for these samples, Li et al. (2016) re-analysed the multi-grain single aliquot data sets for samples HF1, HF3, HF4, HF8, HF10 and HF11, covering the entire range of ages for the Middle Trench, and, as a cross-check, included samples HF1 and HF3 which do not have any problems with saturation. These analyses confirm the observations of Douka et al. (2014) that aliquots from the same and different samples exhibit a wide range of dose response curve shapes and characteristic saturation dose (D_0) levels. Li et al. (2016) also determined that the single aliquot dose response curves could be divided into three broad groups (‘early’, ‘medium’ and ‘later’), with each group saturating at a different dose level (Fig. 7a). The ‘early’ group saturated at low doses (<100 Gy), the ‘later’ group at much higher dose levels (>270 Gy) and the

'medium' group at intermediate doses. They found that each group of dose response curves could be well-defined by a standardized growth curve (SGC) (e.g., Roberts and Duller, 2004; Li et al., 2015a). The three SGCs were identical up to a dose of 50 Gy, after which they started to deviate significantly (Fig. 7b).

Li et al. (2016) calculated D_e values for each group ('early', 'medium' and 'later') and for each of the six samples in two different ways: 1) using the full single aliquot regenerative-dose (SAR) dose response curves for each multi-grain aliquot; and 2) using the SGC for each group. They used the central age model (CAM) of Galbraith et al. (1999) to obtain a weighted mean D_e value for each group in each sample (Li et al., 2016: Table 4). The corresponding ages are presented in Table 1 here, together with the previously published single aliquot ages obtained from the same data, and the single grain ages obtained from a different subset of grains (Douka et al., 2014). For the two samples (HF1 and HF3) with D_e values of ≤50 Gy (i.e., the region of the dose response curve that is identical for all three groups of aliquots: Fig. 7b), all age estimates are statistically consistent, regardless of method of analysis. For the remaining samples with D_e values of ≥100 Gy (HF4, HF8, HF10, HF11), all SAR and SGC ages obtained for the 'early' group are underestimated significantly compared to the ages obtained for the 'medium' and 'later' groups. For these samples, >60% of the aliquots in the 'early' group were fully saturated (Li et al., 2016: Table 3), so finite D_e values could not be obtained. This resulted in a truncated D_e distribution and an underestimation of the true sample mean D_e and corresponding age (italicized values in Table 1). The ages for the 'medium' and 'later' groups are consistent with each other and with the previously published single aliquot and single grain ages. We consider the most reliable ages for these samples are those estimated from the 'later' group (highlighted in bold and grey in Table 1), as these are not affected by saturation issues within the range of doses relevant to D_e estimation. Consequently, the latter provide the most robust quartz OSL ages for comparison with the ages obtained from K-feldspars in this study.

While we are confident in the reliability of the OSL ages for these lower samples from the Middle Trench, the impact of saturation on the estimation of D_e prohibits the determination of quartz OSL ages for the older sediments in the Deep Sounding. An alternative approach needed to be investigated for these deposits, as described below.

The infrared stimulated luminescence signal from K-feldspar grains

Compared to the OSL signal from quartz, the IRSL signal from K-feldspars is usually saturated at much higher doses, enabling much higher finite D_e values (and thus older ages) to be measured. Sand-sized K-feldspar grains also receive a high contribution to the total dose rate from the radioactive decay of ^{40}K and ^{87}Rb inside their crystal lattices. This higher internal dose rate reduces the effect of any spatial or temporal inhomogeneity in the external beta and gamma dose rates, and variations in water content, on the total dose rate. However, feldspars have long been known to exhibit a phenomenon called 'anomalous fading' (Wintle, 1973; Spooner, 1992, 1994; Aitken, 1998; Huntley and Lamothe, 2001; Huntley and Lian, 2006): the leakage of electrons from traps at a much faster rate than would be expected from kinetic considerations. If this fading is not detected and corrected (e.g., Huntley and Lamothe, 2001), then ages can be significantly underestimated. Recent progress in understanding anomalous fading in feldspar has raised the prospect of isolating a non-fading IRSL component, or one less prone to fading; Li et al. (2014b) provided an overview of current methods. Isolation of a suitable dating signal can be achieved by first bleaching the feldspar grains using infrared photons at 50°C and then measuring the post-infrared IRSL (pIRIR) signal at an elevated temperature (>200°C) (Thomsen et al., 2008; Buylaert et al., 2009; 2012; Thiel et al., 2011). An alternative approach is to measure the pIRIR signal at a series of successively raised temperatures, from 50 to 300°C, using the so-called multiple-elevated-temperature pIRIR (MET-pIRIR) procedure of Li and Li (2011, 2012) or the pre-dose MET-pIRIR (pMET-pIRIR) procedure of Li et al. (2014a), which are capable of isolating signals that do not fade or that fade negligibly.

Sample collection, preparation and equipment for IRSL measurement

Two sediment samples for luminescence dating were collected in April 2012 from a west-facing temporary section in the Trench S excavation, and 12 samples were collected in September 2012 from the south-facing wall of the Deep Sounding. The stratigraphic positions and contexts of all samples are shown in Fig. 4. At each sampling location tubes (each about 5 cm in diameter and 15 cm long) were hammered into the cleaned section face, avoiding mole rat burrows visible in the exposed section.

Sample preparation was identical to that described in Douka et al. (2014) except that separated feldspar, rather than quartz, fractions were used, and different grain-size ranges were selected for dating different samples based on what size fraction was available. Sand-sized grains were commonly scarce in all samples. The K-feldspar grains were extracted using a sodium polytungstate solution of 2.55 g/cm^3 and were then etched using 10% HF acid for 40 min to clean the surfaces of the grains and to reduce the thickness of the external alpha-irradiated layer.

The IRSL measurements were made on an automated Risø TL-DA-20 luminescence reader equipped with IR diodes (870Δ40 nm) for stimulation of K-feldspars (Bøtter-Jensen et al., 2003) and a calibrated ^{90}Sr/^{90}Y beta source for irradiations. The IRSL signals were detected by an Electron Tubes Ltd 9235QA photomultiplier tube with the stimulated luminescence passing through a filter pack containing Schott BG-39 and Corning 7-59 filters, which provide a UV/blue transmission window (320–480 nm). All multi-grain measurements were made using 9.8 mm-diameter stainless steel discs with the central 5 mm coated with "Silkospray" silicone oil to adhere a monolayer of several hundred grains to the surface of each disc ('aliquot').

MET-pIRIR and pMET-pIRIR measurements and results

We measured the D_e values for the oldest samples from the Middle Trench (HF4, HF8, HF10 and HF11) and the underlying older samples from the Deep Sounding using single aliquots composed of sand-sized grains of K-feldspar and the MET- and pMET-pIRIR dating procedures. IRSL signals were measured by progressively increasing the stimulation temperature from 50 to 250°C in 50°C steps (Table 2a). A preheat of 300°C for 60 s was applied prior to measurement of the natural, regenerative and test dose signals, and a test dose of 64 Gy was used for all samples. The resulting signals were calculated as the sum of counts over the initial 10 s of infrared stimulation, with a 'late light' subtraction (Aitken, 1998) of the background count rate over the final 10 s of stimulation. For each IRSL measurement, an 'IR-off' period up to 50 s was applied to monitor and minimize the isothermal decay signal (Fu et al., 2012). MET-pIRIR signals obtained at elevated temperatures (>200°C) show negligible rates of anomalous fading and require no fading correction (Li and Li, 2011, 2012; Li et al., 2014b).

For the samples collected from the Deep Sounding we applied the pre-dose MET-pIRIR (pMET-pIRIR) procedure (Li et al., 2014a) to obtain D_e values for the multi-grain aliquots of K-feldspar. This procedure differs slightly from the conventional MET-pIRIR procedure in that the high-temperature infrared bleach (or 'hot' bleach) applied at the end of each SAR cycle (Step 15 in Table 2a) is replaced by a solar simulator bleach for ~2 hr (Step 15 in Table 2b). The former is used to minimize any residual IRSL signal that may have accumulated from the previous SAR cycle, whereas the latter has been shown to 'reset' the dose-dependent sensitivity of the MET-pIRIR signals (Li et al., 2013a, 2014a). As a result, the pMET-pIRIR procedure negates the need to correct for sensitivity change between measurement cycles. Each of the L_x, T_x and L_x/T_x (and L_n, T_n and L_n/T_n) IRSL signals (Table 2b) can, therefore, be used to estimate D_e values.

Decay curves and dose response curves for K-feldspar

Fig. 8 shows the IRSL (50°C) and MET-pIRIR (100–250°C) decay curves for a natural aliquot of sample HF6021. Similar decay curve shapes are observed for all samples, with the intensities of the MET-pIRIR signals ranging from a few hundred to a few thousand counts per second.

We tested whether the SGC method, which was first proposed by Roberts and Duller (2004) and further developed by Li et al. (2015a, b), could be used to reduce instrument time, given the long irradiations required for these samples. Li et al. (2015b) observed that the non-fading MET-pIRIR signals of K-feldspars from different regions of the world share a common dose response curve (DRC) if they are appropriately normalized using one of the regenerative dose signals. This procedure is called regenerative-dose normalisation or 're-normalisation' (Li et al., 2015a, 2015b). To test its applicability to the samples from the Haua Fteah, we plotted the re-normalized DRCs for the L_x/T_x and L_x signals from three samples (HF6019, HF6021 and HF6023) measured at different stimulation temperatures (Fig. 9). The DRCs were constructed using a series of regenerative doses, ranging from 220 to 1110 Gy, including a duplicate dose to determine the recycling ratio for the L_x/T_x signal (or the reproducibility ratios for the L_x and T_x signals; Li et al., 2014a) and a zero dose (0 Gy) to determine the extent of recuperation for each of the signals. The data sets for each of the DRCs were then re-normalized to unity at a dose of 440 Gy. The recycling (and

reproducibility) ratios for all aliquots are within 10% from unity, and the recuperation levels are less than 8% and 5% for the L_x/T_x and L_x signals at 250°C, respectively, thus satisfying the acceptance criteria for sample suitability. Due to the relatively dim IRSL sensitivity of the Haua Fteah samples (Fig. 8) and the small dose-response range in the T_x signal (Li et al., 2014a, 2014b), we observed a large scatter in the DRCs constructed from the T_x signals, so we focused on the L_x/T_x and L_x signals only.

The signals measured at different stimulation temperatures produced L_x/T_x DRCs that differ in shape (Fig. 9, left-hand column). The 50°C IRSL signal (the stippled line in Fig. 9a) has the highest saturation dose level, whereas those for the 200 and 250°C signals (the stippled lines in Fig. 9g and i) saturate at lower doses; the solid lines in panels a, c, e and g are the best-fit curve to the 250°C data (the stippled line in panel i), and illustrate the gradual decline in saturation level with increasing stimulation temperature. Each of the DRCs in Fig. 9 could be fitted using a single saturating-exponential function of the form $I = I_0(1\text{-}\exp^{-D/D}{}_0) + y_0$, where I is the L_x/T_x value at regenerative dose D, I_0 is the saturation value of the exponential curve, D_0 is the characteristic saturation dose and y_0 is a constant. The D_0 values obtained by fitting the data sets for the L_x/T_x signals decrease from 497 Gy at 50°C to 352 Gy at 250°C, respectively, whereas the shapes of the re-normalized DRCs for the sensitivity-uncorrected signal L_x (Fig. 9, right-hand column) are indistinguishable at different stimulation temperatures and yield a common D_0 value of ~512 Gy. This finding is consistent with observations made in previous studies (Li et al., 2013a; Chen et al., 2015; Guo et al., 2015) and suggests that the L_x signal could be used to measure to much higher doses (>1000 Gy) than can be achieved using the L_x/T_x signal, and especially at the highest stimulation temperature (250°C) which is associated with the non-fading pMET-pIRIR signal.

Another key feature of Fig. 9 is that all three samples share similar DRCs for each of the L_x/T_x and L_x signals, suggesting that SGCs can be established for K-feldspar from the Haua Fteah. To validate the applicability of D_e estimation based on the SGCs in Fig. 9, we compared the SGC D_e values of the L_x/T_x and L_x signals at 250°C with the SAR D_e values obtained at a stimulation temperature of 250°C from full DRCs for aliquots of samples HF6019, HF6021 and HF6023 (Fig. 10). The SGC and SAR D_e values so obtained are statistically consistent at 2σ (Fig. 10a and c). The same data are also displayed as radial plots of the ratios of the SGC to SAR D_e values. All ratios are consistent with unity at 2σ for both

the L_x/T_x (Fig. 10b) and L_x (Fig. 10d) signals. On the basis of this result, D_e values for all samples were obtained by measuring only the natural signal (L_n), one regenerative dose signal (L_x) and the corresponding test dose signals (T_n and T_x) for each aliquot. The re-normalized natural pMET-pIRIR signals were then projected onto their corresponding SGCs to determine individual D_e values for each aliquot; see Li et al. (2015a, 2015b) for a full description of D_e determination using SGCs.

Residual dose, dose recovery and anomalous fading tests

We conducted several internal tests—including dose recovery, anomalous fading and residual dose tests—to check whether the pMET-pIRIR L_x/T_x and L_x signals can produce reliable D_e estimates for the Haua Fteah samples. For the residual dose test, four aliquots from nine of the samples (HF4, HF8, HF10, HF6008, HF6009, HF6017, HF6021, HF6029 and HF6035) were bleached for ~4 hr using a UVACUBE 400 solar simulator. A bleaching time of 4 hr was chosen as it has proven sufficient to reach a stable residual dose in tests on other samples (e.g., Li and Li, 2011; Li et al., 2014b). The residual doses were then estimated by measuring the bleached aliquots with the conventional MET-pIRIR procedure outlined in Table 2a; the use of a 'hot' bleach, rather than a 2 hr simulator bleach, was given at step 15 for practical reasons (following Guo et al., 2015). The residual doses obtained for the 250°C MET-pIRIR signal range from 5 to 21 Gy for these samples, and are plotted against the corresponding D_e values for each of the samples in Fig. 11 (the D_e estimates are discussed below). There is a positive correlation between residual dose and D_e, which is similar to observations made previously (e.g., Sohbati et al., 2012). This may be the result of either thermal transfer (Buylaert et al., 2012) or the dose dependency of the non-bleachable signal (Li et al., 2013b). We consider the intercept of 3.1 ± 1.3 Gy on the y-axis to be the closest approximation to the true residual dose for the samples from the Haua Fteah (following Sohbati et al., 2012). Although this value is negligible compared to the D_e values of the Deep Sounding and Trench S samples, we subtracted this residual dose value from the final D_e value for each sample before calculating the final ages.

Dose recovery tests (Galbraith et al., 1999) were performed on three of the samples (HF6019, HF6021 and HF6043). Four aliquots each from HF6019 and HF6021, and eight aliquots from HF6043, were bleached for ~4 hr using the solar simulator and then given a

beta dose of 550 Gy (HF6019), 370 Gy (HF6021), 420 Gy or 210 Gy (HF6043), the latter to check for any dependency on size of dose. The given doses were treated as surrogate 'natural' doses and measured using the pMET-pIRIR procedure in Table 2b. A residual dose was subtracted from the measured (recovered) doses at each stimulation temperature, and the measured dose to the given dose was calculated for the various L_x/T_x and L_x signals. These ratios are plotted as a function of stimulation temperature in Fig. 12a–d. For all three samples, the measured/given dose ratios are consistent with unity at 2σ for the 200 and 250°C signals, demonstrating that given (known) doses of 210–550 Gy can be recovered successfully using the pMET-pIRIR procedure under controlled laboratory conditions, and that the 200 and 250°C pMET-pIRIR signals (L_x/T_x and L_x) should be reliable for D_e estimation.

We conducted fading tests on six aliquots of sample HF6021 using a single-aliquot procedure similar to that described by Auclair et al. (2003), but based on the MET-pIRIR procedure in Table 2a. Doses of 220 Gy were administered using the laboratory beta source, and the irradiated aliquots were then preheated and stored for periods of up to a week at room temperature. The time of prompt measurement ranged from ~1720 s for the 50°C IRSL signal to ~2500 s for the 250°C MET-pIRIR signal. For practical reasons, a 'hot' IR bleach was used instead of a solar simulator bleach at the end of each SAR cycle, but this choice should not affect the outcome of the fading test. Fig. 13 shows the fading measurement results and resulting *g*-values for the IRSL and MET-pIRIR L_x/T_x signals. The *g*-values decrease as the stimulation temperature increases, falling to values consistent with zero for the signals measured at 200 and 250°C; these fading data have large uncertainties due to the relatively dim signals of the sample and the low fading rates at elevated temperatures. These results suggest that the MET-pIRIR procedure is capable of isolating the non-fading signals for the Haua Fteah samples.

Equivalent dose estimates

Based on the above performance tests, the MET-pIRIR and pMET-pIRIR procedures in Table 2 were used to estimate the D_e values for the Haua Fteah samples. Ten aliquots were measured for each sample. The four youngest samples (HF4, HF8, HF10 and HF11) were measured using the conventional MET-pIRIR procedure and the full SAR sequence (Table 2a). The other 14 samples were measured using the pMET-pIRIR procedure (Table 2b). For

three of these samples (HF6019, HF6021 and HF6023), we used the full SAR procedure to establish individual DRCs (Fig. 9). For the remaining 11 samples, the natural signal, one regenerative-dose signal and the corresponding test dose signals were measured and their D_e values estimated based on the SGC curves in Fig. 9.

The weighted mean D_e values and standard errors for ten aliquots of each sample were calculated using the central age model (CAM) (Galbraith et al., 1999; Galbraith and Roberts, 2012). The weighted mean D_e values for the L_x/T_x signals (filled circles) and L_x signals (open squares) are plotted as a function of stimulation temperature in Fig. 14. For each sample, the L_x/T_x and L_x signals are statistically consistent, regardless of stimulation temperature. The D_e values increase with stimulation temperature and, for most samples, statistically consistent D_e values (the dashed line in Fig. 14) are obtained for the highest temperatures (200 and 250°C). This consistency in D_e values indicates that a non-fading component is present at these elevated temperatures, and serves as an internal diagnostic tool to validate the isolation of a stable, non-fading signal for age determination (Li and Li, 2011). Final ages are based on the D_e values obtained from the L_x/T_x signals at 250°C for samples HF4, HF8, HF10 and HF11, and the weighted mean of the D_e estimates obtained from the L_x/T_x and L_x signals at 250°C for the other samples (Table 3).

Environmental dose rate measurements and results

The total environmental dose rate to acid-etched sand-sized grains of K-feldspar consists of contributions from beta, gamma and cosmic radiation external to the grains, and a significant internal beta dose rate from the radioactive decay of ^{40}K and ^{87}Rb.

The external beta dose rates for all samples were measured directly by measuring dried, homogenized and powdered samples in the laboratory, using a GM-25-5 low level beta counter (Bøtter-Jensen and Mejdahl, 1988). We prepared and measured samples, analysed the resulting data, and calculated beta dose rates and errors following the procedures described and tested in Jacobs and Roberts (2015). GM-25-5 counting is our method of choice for beta dose rate determination because it is less sensitive to potential inaccuracies arising from U disequilibrium than other methods that measure only the parental U concentration (e.g., ICP-MS). Numerical modelling has shown that even the most common time-dependent disequilibria in the ^{238}U series are unlikely to give rise to errors in

the total dose rate of more than 2–3% when emission-counting techniques, such as GM-25-5 beta counting, are employed (Olley et al., 1996, 1997). For all samples, allowance was made for the effects of grain size (Mejdahl, 1979) and hydrofluoric acid etching (Bell and Zimmerman, 1978) on beta-dose attenuation.

The gamma dose rates for the Deep Sounding samples were measured directly at each sample location at the time of sample collection, using a NaI(Tl) detector, calibrated at the Research Laboratory for Archaeology and the History of Art, University of Oxford (Rhodes and Schwenninger, 2007). This equipment was not available when the Trench S samples were taken, so background sediment samples were used. The gamma dose rates were calculated based on the K, U and Th concentrations obtained from the gamma-ray spectra, and then converted to gamma dose rates using the conversion factors of Guérin et al. (2011). This approach takes into account spatial heterogeneity in the gamma radiation field (a radius of ~40 cm) around each sample.

By measuring the external beta and gamma dose rates in these ways, we have implicitly assumed that the present state of (dis)equilibrium in the U and Th decay chains has prevailed throughout the period of sample burial. These dose rates were corrected for the measured (field) water content of each sample. For the latter, we collected sediment at the rear of each sample hole, ~20 cm into the section wall, and away from the desiccated faces of the excavation. We assume that these field values are representative of the average long-term water contents of the sediments, but note that the effect of changes in moisture content on dose rate to K-feldspar grains is small (~0.5% decrease in dose rate for each 1% increase in water content), because the internal dose rate is not affected by water content. We assigned a relative uncertainty of ± 20% (at 1σ) to accommodate any likely variations over the burial period.

The internal beta dose rate was calculated by assuming internal ^{40}K and ^{87}Rb concentrations of 10 ± 2% (Smedley et al., 2012) and 400 ± 100 µg/g (Huntley and Hancock, 2001), respectively. These concentrations were converted to dose rates (Guérin et al., 2011) and corrected for the absorbed dose fraction, which varies depending on the diameter of the dated grains. For K-feldspar grains of 90–125 µm diameter, this yields an effective internal beta dose rate of 0.39 ± 0.09 Gy/ka, increasing to 0.67 ± 0.15 Gy/ka for grains of 180–212 µm in diameter. The internal dose rates comprise 11–25% of the total dose rates.

The cosmic-ray dose rates were estimated from the equations provided by Prescott and Hutton (1994), taking into account the burial depth of each sample (averaged over the entire period of burial), the thickness of limestone above each sample (~14 m), the density of the sediment and rock overburden, and the altitude (~57 m) and geomagnetic latitude (31.9°) of the site. We also took into consideration the zenith angular distribution of cosmic rays (Smith et al., 1997) to allow for the configuration of the cave.

The dose rate results for the samples from Haua Fteah are provided in Table 3. The total dose rates span a relatively large range, from 2.27 ± 0.13 (HF11) to 3.63 ± 0.19 (HF6019) Gy/ka. For all samples, the uncertainty associated with the total dose rate represents the quadratic sum of all known and estimated sources of random and systematic error.

Results

Age estimates and comparisons

The D_e and dose rate information for the four samples for which we measured both the quartz OSL and K-feldspar 250°C MET-pIRIR signals are presented in Table 3; details of the D_e values and dose rates for the quartz samples are provided in Douka et al. (2014) and Li et al. (2016), and the OSL ages are listed in Table 1. The most reliable single aliquot OSL ages (shown in bold and grey cells in Table 1) and single grain OSL ages (also shown in Table 1) are statistically consistent with their corresponding MET-pIRIR ages at 1σ (samples HF4, HF8 and HF11) or 2σ (sample HF10). In contrast to the small multi-grain aliquots (8–15 grains per aliquot; Douka et al., 2014) and single grain OSL measurements on quartz, the MET-pIRIR D_e values were obtained from the simultaneous measurement of hundreds of K-feldspar grains per aliquot; these 'grain-average' results were subsequently used to calculate the final D_e values and ages.

The agreement between the single grain and single aliquot quartz OSL ages and the single aliquot K-feldspar MET-pIRIR ages has five important implications:

1) Incomplete bleaching of the OSL and pIRIR signals is not significant. The MET-pIRIR 250°C signal requires a longer sunlight exposure time than the OSL signal to empty the relevant electron traps and reset the 'clock' (e.g., Li et al., 2014b), so the similarity in ages

suggests that the quartz and K-feldspar signals were reset completely at the time of sediment deposition in the Haua Fteah.

2) The effect of small-scale differences in beta dose rate delivered to individual quartz grains, and the rejection of physically unsuitable single grains on the basis of their malign OSL behaviours, have not introduced any bias to the single grain OSL chronology presented in Douka et al. (2014) (Fig. 3).

3) It is possible to calculate reliable ages from OSL signals that are close to dose saturation for single aliquots and single grains of quartz that have dose response curves with sufficiently high characteristic saturation dose levels (Li et al., 2016).

4) The agreement between the single grain OSL, multi-grain single aliquot OSL and MET-pIRIR ages for sample HF8, and their discrepancy with the age of the tephra shards identified from the same context, support our previous interpretation (Douka et al., 2014) that there was a significant hiatus in sediment deposition between ~70 and 50 ka. Whether this is true across the entire site, or applies only to the area from where the samples were collected, remains to be investigated. This hiatus was not taken into consideration in the Bayesian model presented in Douka et al. (2014).

5) The agreement among the various age estimates for samples HF4, HF8, HF10 and HF11 gives confidence in the pMET-pIRIR ages for the samples from the Deep Sounding and Trench S.

The final ages for these samples are listed in Table 3 together with the supporting D_e and dose rate estimates. Uncertainties on the ages are given at 1σ (standard error on the mean) and were derived by combining, in quadrature, all known and estimated sources of random and systematic error.

Discussion

The optical ages of 150 ± 10 (HF6009) and 153 ± 10 ka (HF6008) for the lowermost exposed levels in Trench S date the earliest evidence for human activity in the Haua Fteah. These ages are consistent with the age of 149 ± 10 ka (HF6017) for sediments from the overlying base of McBurney's Deep Sounding, and suggest that the lowest ~1 m of deposit overlying the rockfall at the base of the current excavations was deposited near the end of MIS 6. Although pollen is very poorly preserved in the Trench S sediments, an abundant and

diverse molluscan fauna, including *Bellamya* sp., *Helix melanostoma*, *Mastus* sp., *Vitrea* spp., Vitrinidae, *Leiostyla* sp. and other Pupillidae, indicating the presence of semi-permanent water bodies, marsh and scrubland with abundant vegetation, is suggestive of mild and relatively humid conditions. Human presence is attested by fragments of burnt *Patella* and *Phorcus* spp.

Samples HF6019 and HF6043 were both collected from context 832, ~80 cm above sample HF6017. The corresponding ages of 127 ± 11 and 136 ± 10 ka are statistically consistent at 1σ and place deposition of these sediments at around the MIS 6/5 transition. Context 832 corresponds to McBurney's spit 176, which produced the earliest assemblage of "Pre-Aurignacian" lithic cultural remains. The next four overlying samples were collected within 30 cm of each other and 40 cm above HF6019 and HF6043. All four samples derive from layers that produced exceptionally high quantities of "Pre-Aurignacian" lithic artefacts, falling within spits 174/173 (HF6021), 172 (HF6023 and HF6012) and 171/172 (HF6025) (Fig. 15). They have statistically consistent ages of 127 ± 8 (HF6021), 126 ± 10 (HF6023), 121 ± 8 (HF6012) and 119 ± 9 ka (HF6025), suggesting a period of significant occupation of the cave during the MIS 5e interstadial, which peaked at ~123 ka (Lisiecki and Raymo, 2005; Fig. 16). Within the same phase is the occupation represented by very low frequencies of artefacts in McBurney's spits 69 and 66 (Fig. 15), respectively 45 and 95 cm above the culturally-rich "Pre-Aurignacian" horizon that produced statistically consistent ages of 127 ± 9 (HF6027, spit 69) and 119 ± 7 ka (HF6029, spit 66).

A sediment sample (HF6031) collected a further 75 cm above these samples gave an age of 102 ± 9 ka, and two other samples, collected 85 and 105 cm above HF6031, produced ages of 90 ± 5 (HF6045) and 104 ± 7 ka (HF6035). These last three samples are not in strict stratigraphic order, but they are consistent at 2σ. The ages are also consistent with the pollen in these sediments (characterised by diverse maquis and savannah taxa, and rather similar in aspect to early Holocene assemblages) that suggests deposition during a major interstadial, most probably MIS 5c. HF6031 falls within McBurney's spit 61, which produced only a few lithic artefacts (Fig. 15). A slight increase in the frequency of lithic artefacts occurs in the three overlying spits (58–60), as well as in the recently excavated corresponding contexts in Trench D. Although the cultural record at these depths in the Deep Sounding is considerably less artefact-rich in comparison with the lower "Pre-Aurignacian" horizon, it is

noteworthy that this apparent increase in occupation activity appears to coincide with a return to interstadial conditions. Samples HF6045 and HF6035 correlate with McBurney's spits 54–56; while his excavations produced no lithic artefacts from these spits, our excavations of equivalent contexts in Trench D produced very low frequencies of small and fragmented lithic artefacts.

There are low-level signs of human presence through most of the upper ~80 cm of the Deep Sounding, but we have no quartz or K-feldspar ages for this part of the sequence. The uppermost ~20 cm contains pollen indicative of a cool steppe environment and there is a notable increase in the frequency of lithics artefacts (Fig. 15). We suggest that this increase in human presence corresponds to a stadial period, possibly MIS 5b (Fig. 16). The basal sediments of the Middle Trench were dated by Douka et al. (2014) using quartz OSL to 71 ± 7 ka (sample HF11, from McBurney's spit 55-112, Layer XXXIV), and this age has been confirmed in the present study using the MET-pIRIR signal from K-feldspar (73 ± 5 ka). With the start of MIS 4 dated variously to between 74 and 71 ka, it is likely that human activity in the lowermost sediments of the Middle Trench is associated with the MIS 5a interstadial or the onset of MIS 4.

The intensive wet sieving of all excavated sediment employed by the new excavations has found lithic artefacts throughout the Deep Sounding sequence. There are very few at certain depths, however, and they are often minute and fragmentary, and may constitute material that was reworked from the surrounding landscape into the Deep Sounding area. It is tempting to assume that the marked differences in artefact concentrations through the Deep Sounding sequence are a proxy for fluctuations in population size in the local area, but with two important caveats. First, it is possible, indeed likely, that there was spatial variation across the cave floor in the intensity with which artefacts were discarded; artefact-poor layers within the Deep Sounding may preserve larger numbers of artefacts elsewhere in the unexcavated parts of the cave. Further large-scale excavations are required to investigate whether this is the case. Second, a single knapping episode or core reduction sequence within an excavated area might create the impression of a significant human presence yet, in fact, be the result of a brief moment in time and represent the cultural waste of a few individuals. In this instance, we have tried to use the technological components of the assemblage and frequency of lithic refits to clarify

the nature of activities represented. Despite these uncertainties, the most striking finding from the new chronology of the Deep Sounding is the evidence for highly intermittent human use of the cave while these lower sediments were accumulating. Activities occurred primarily during interstadial conditions (MIS 5e and MIS 5c) in the lower and middle portions of the Deep Sounding, and possibly during the MIS 5b stadial in the undated uppermost ~20 cm of the Deep Sounding sequence.

Conclusions

The evidence of minute quantities of lithic debitage in the Trench S sediments, combined with the new optical ages obtained using K-feldspars from the Deep Sounding, suggest that humans may have first visited the Haua Fteah near the end of MIS 6. Moving upwards through the Deep Sounding, a very sharp increase in lithic artefact densities—the first main phase of "Pre-Aurignacian" occupation—clearly corresponds to a period of extensive use of the cave. It is concentrated around the MIS 5e climatic optimum and drops off towards the end of this sub-stage (Figs. 15 and 16). No other periods of "Pre-Aurignacian" occupation are as rich as this early phase, which is succeeded by only a hint of human presence that possibly corresponds to the end of MIS 5e and/or MIS 5d. The second clear phase of human activity occurs in the middle of the Deep Sounding sediments and appears to date to the MIS 5c interstadial. While artefact frequencies remain low, it is a relatively prominent occupation horizon in comparison to the dearth of artefacts in the underlying and overlying sediments. After another period of exceptionally low artefact densities in the overlying undated layers, there is a notable increase in human presence in the uppermost ~20 cm of the Deep Sounding that remains undated but possibly corresponds to the MIS 5b stadial (based on the pollen composition). There is no break in artefact densities between the top of the Deep Sounding and the base of the Middle Trench. Although the possibility of intervening sedimentary hiatuses needs to be considered, the field evidence suggests continuity in occupation from the final phase of the "Pre-Aurignacian" to the artefact-rich "Levalloiso-Mousterian" layers at the base of the Middle Trench, which date to MIS 5a and the onset of MIS 4.

Reynolds (2013) suggested that the "Pre-Aurignacian" might be a littoral facies of a Levallois-based MSA in northeast Africa, and it is notable that the new excavations have

found evidence for marine gathering (molluscs, crabs) and fishing, as well as terrestrial mammal hunting associated with the "Pre-Aurignacian" lithics in the Deep Sounding. He also raised the possibility that the distinction between "Pre-Aurignacian" and "Levalloiso-Mousterian" 'industries' could simply be a product of sampling, given that the former derives from ~35 m^3 of sediment excavated from the Deep Sounding compared with ~120 m^3 of the lower Middle Trench from which the latter derives. Jones (2016), however, found significant differences between the core morphologies and technologies of these two MSA assemblages that are unlikely to result from sampling bias, with the "Pre-Aurignacian" sharing more similarities in these aspects with the Later Stone Age "early Dabban". The "Levalloiso-Mousterian" has a more formal and consistent approach to reduction, a greater preponderance of disc and Levallois cores, cores used to produce points as well as flakes, and examples of cores used as scrapers and Levallois cores use to produce points as well as flakes. Nevertheless, the two MSA assemblages share a number of similarities, including: Levallois technology; blades, bladelets and elongated flakes, with a predominance of flakes; hard hammer reduction on unprepared platforms; and a dominance of burins, notches and scrapers in the retouched categories. The exploitation of the products of reduction remains similar between the two industrial forms, so overall use of lithics in the ecology of the groups appears to have been similar too. The "Levalloiso-Mousterian" can be ascribed with confidence to *Homo sapiens*, given the presence of two modern human jaws near its base (in Layer XXXIII, which has a modelled age of 73–65 ka: Douka et al., 2014). It is parsimonious to conclude that the makers of the "Pre-Aurignacian" were also *Homo sapiens* given the fundamental similarities in lithic technologies and subsistence data, as well as evidence of shell-working (currently under study by EH and CH) associated with the "Pre-Aurignacian" occupation of the cave.

Homo sapiens fossils have been found at a number of sites in the Sahara and the Maghreb associated with Aterian technologies, which included tanged points and bifacial foliates that are quite different from the "Pre-Aurignacian" (Wrinn and Rink, 2003; Trinkaus, 2005; Nespoulet et al., 2008; Barton et al., 2009; Scerri, 2013). The Saharan ages for these sites range between ~60 and 80 ka, whereas those in the Maghreb go back as far as 145 ± 9 ka at Ifri n'Ammar (Richter et al., 2010). In Cyrenaica, Aterian 'type fossils' were recorded at the Hagfet et Tera cave near Benghazi (McBurney and Hey, 1955) and a single tanged point

was found on the surface near the Haua Fteah (Reynolds, 2013), but there is no evidence for Aterian technologies in the excavations at the Haua Fteah (Reynolds, 2013; Scerri, 2013). The chronologies currently available for Aterian sites do not allow us to determine whether these technologies originated in sub-Saharan Africa, the Sahara or the Maghreb, although it is commonly argued that modern humans with Aterian technologies likely dispersed into North Africa during humid phases within MIS 5, across what was then the 'Green Sahara' (e.g., Osborne et al., 2008; Barton et al., 2009; Garcea, 2010; Drake et al., 2011, 2013). The new optical ages for the Deep Sounding of the Haua Fteah provide prima facie evidence that modern humans equipped with a "Pre-Aurignacian" MSA technology were in Cyrenaica at least as early as modern humans with Aterian technologies were present in the Maghreb.

Whilst research into the movement of modern humans out of Africa has dominated discussions, the role of different populations within Africa and variation in their ecological and cultural backgrounds remain relatively unexplored. The implication of the present study is that a diverse group of populations probably originating from different parts of sub-Saharan Africa filtered through the humid Sahara during the latter stages of MIS 6 and early MIS 5. One group used Aterian lithic technologies and another used the "Pre-Aurignacian". Yet others may have derived from the Nile corridor and used Nubian industries (Van Peer, 1991; Schild and Wendorf, 1993; Van Peer and Vermeersch, 2007; Vermeersch, 2010). Isolation and extinction amongst these groups would have been likely, as indeed the degree of variability seen in the lithic record suggests, with only the Aterian and Nubian industries showing wider spatial patterning. The "Pre-Aurignacian" of Cyrenaica may have developed locally into the "Levalloiso-Mousterian" but it could equally derive from the Aterian or Nubian forms. The poverty of the record from the Sahara and sub-Saharan regions remains a major problem to investigating these important questions.

McBurney used the term "Pre-Aurignacian" because of the similarities he saw with Pre-Aurignacian (also known as Amudian) blade-based industries in Southwest Asia, notably at Jabrud in Syria (Rust, 1950) and Tabun in Israel (Garrod, 1937). He thought these links suggested "an exotic extra-African origin for the newly discovered complex" (McBurney, 1967: 93). The Pre-Aurignacian (Amudian) industries of Southwest Asia (part of the Acheulo-Yabrudian Cultural Complex) date to around 400–200 ka at Qesem Cave (Barkai et al., 2009). These are notably older than the Libyan Pre-Aurignacian, so cultural or demographic links

between these Levantine groups and the occupants of the Haua Fteah in MIS 5e are not supported by the dating evidence presented here. The question remains open, therefore, of the dispersal routes that brought the first modern humans to Cyrenaica, with the Sahara, Nile valley and indeed the Levant all being potential candidates. Perhaps more important in terms of future research, however, is understanding the nature of and reasons for the evident variability in MSA lithic technologies used by modern humans across North Africa from—on the evidence of the new ages for the Haua Fteah—the earliest phases of their presence in the region.

Acknowledgements

We thank in particular the Department of Antiquities of Libya for permission to undertake the new excavations at the Haua Fteah, and for logistical support for the fieldwork. The project was initially termed the Cyrenaican Prehistory Project, with the excavation permit arranged by and funding provided by the Society for Libyan Studies, whose support is gratefully acknowledged. From 2009, it has also been termed the TRANS-NAP project from the acronym of the European Research Council grant to GB (Advanced Investigator Grant 230421: “Cultural Transformations and Environmental Transitions in North African Prehistory”), which provided the major funding for the project and is also gratefully acknowledged. We thank Simon Armitage (Department of Geography, Royal Holloway London) for the loan of the gamma spectrometer for in situ background radiation measurements and the analysis of those data. The optical dating research program was funded by the Australian Research Council through Discovery Project DP1092843 to Jacobs, Future Fellowship FT140100384 to Li, and Laureate Fellowship FL130100116 to Roberts. Yasaman Jafari and Terry Lachlan are thanked for laboratory support. Contributor roles: ZJ, BL, RGR: optical dating; LF, CH, SJ: stratigraphic analysis; EH, CH: molluscan analysis; SJ, TR: artefact analysis; DS, CH: palynology; GB: project director.

References

Aitken, M.J., 1998. An Introduction to Optical Dating. Oxford University Press, Oxford.

Auclair, M., Lamothe, M., Huot, S., 2003. Measurement of anomalous fading for feldspar IRSL using SAR. Radiat. Meas. 37, 487–492.

Barkai, R., Lemorini, C., Shimelmitz, R., Lev, Z., Stiner, M.C., Gopher, A. 2009. A blade for all seasons? Making and using Amudian blades at Qesem Cave, Israel. Hum. Evol. 24, 57-75.

Barker, G., Hunt, C., Reynolds, T., 2007. The Haua Fteah, Cyrenaica (northeast Libya): renewed investigations of the cave and its landscape, 2007. Libyan Studies 38, 93-114.

Barker, G., Basell, L., Brooks, I., Burn, L., Cartwright, C., Cole, F., Davison, J., Farr, L., Hamilton, R., Hunt, C., Inglis, R., Jacobs, Z., Leitch, V., Morales, J., Morley, I., Morley, M., Pawley, S., Pryor, A., Rabett, R., Reynolds, T., Roberts, R., Simpson, D., Stimpson, C., Touati, M., der Veen, M., 2008. The Cyrenaican Prehistory Project 2008: the second season of investigations of the Haua Fteah cave and its landscape, and further results from the initial 2007 fieldwork. Libyan Studies 39, 175–222.

Barker, G., Antoniadou, A., Barton, H., Brooks, I., Candy, I., Drake, N., Farr, L., Hunt, C., Ibrahim, A.A., Inglis, R., Jones, S., Morales, J., Morley, I., Mutri, G., Rabett, R., Reynolds, T., Simpson, D., Twati, M., White, K., 2009. The Cyrenaican Prehistory Project 2009: the third season of investigations of the Haua Fteah cave and its landscape, and further results from the 2007–2008 fieldwork. Libyan Studies 40, 1–41.

Barker, G., Antoniadou, A., Armitage, S., Brooks, I., Candy, I., Connell, K., Douka, K., Drake, N., Farr, L., Hill, E., Hunt, C., Inglis, R., Jones, S., Lane, C., Lucarini, G., Meneely, J., Morales, J., Mutri, G., Prendergast, A., Rabett, R., Reade, H., Reynolds, T., Russell, N., Simpson, D., Smith, B., Stimpson, C., Twati, M., White, K., 2010. The Cyrenaican Prehistory Project 2010: the fourth season of investigations of the Haua Fteah cave and its landscape, and further results from the 2007–2009 fieldwork. Libyan Studies 41, 63–88.

Barker, G., Bennett, P., Farr, L., Hill, E., Hunt, C., Lucarini, G., Morales, J., Mutri, G., Prendergast, A., Pryor, A., Rabett, R., Reynolds, T., Twati, M., 2012. The Cyrenaican Prehistory Project 2012: the fifth season of investigations of the Haua Fteah cave. Libyan Studies 43, 115–136.

Barton, R.N.E., Bouzouggar, A., Colcutt, S.N., Schwenniger, J.-L., Clark-Balzan, L., 2009. OSL dating of the Aterian levels at Dar-es-Soltan I (Rabat, Morocco) and implications for the dispersal of modern *Homo sapiens*. Quaternary Sci. Rev. 28, 1914–1931.

Bell, W.T., Zimmerman, D.W., 1978. The effect of HF acid etching on the morphology of quartz inclusions for thermoluminescence dating. Archaeometry 20, 63–65.

Bøtter-Jensen, L., Mejdahl, V. 1988. Assessment of beta dose-rate using a GM multicounter system. Nucl. Tracks Rad. Meas. 14, 187–191.

Bøtter-Jensen, L., Andersen, C.E., Duller, G.A.T., Murray, A.S. 2003. Developments in radiation, stimulation and observation facilities in luminescence measurements. Radiat. Meas. 37, 535–541.

Buylaert, J.P., Murray, A.S., Thomsen, K.J., Jain, M. 2009. Testing the potential of an elevated temperature IRSL signal from K-feldspar. Radiat. Meas. 44, 560–565.

Buylaert, J.P., Jain, M., Murray, A.S., Thomsen, K.J., Thiel, C., Sohbati, R., 2012. A robust feldspar luminescence dating method for Middle and Late Pleistocene sediments. Boreas 41, 435–451.

Chapot, M.S., Roberts, H.M., Duller, G.A.T., Lai, Z.P., 2012. A comparison of natural- and laboratory-generated dose response curves for quartz optically stimulated luminescence signals from Chinese loess. Radiat. Meas. 47, 1045–1052.

Chen, Y.W., Li, S.-H., Li, B., Hao, Q., Sun, J., 2015. Maximum age limitation in luminescence dating of Chinese loess using the multiple-aliquot MET-pIRIR signals from K-feldspar. Quat. Geochronol. 30, 207–212.

De Vivo, B., Rolandi, G., Gans, P.B., Calvert, A., Bohrson, W.A., Spera, F.J., Belkin, H.E., 2001. New constraints on the pyroclastic eruptive history of the Campanian volcanic plain (Italy). Mineral. Petrol. 73, 47–65.

Douka, K., Jacobs, Z., Lane, C., Grün, R., Farr, L., Hunt, C., Inglis, R.H., Reynolds, T., Albert, P., Aubert, M., Cullen, V., Hill, E., Kinsley, L., Roberts, R.G., Tomlinson, E.L., Wulf, S., Barker, G., 2014. The chronostratigraphy of the Haua Fteah cave (Cyrenaica, Northeast Libya). J. Hum. Evol. 66, 39–63.

Drake, N.A., Blench, R.M., Armitage, S.J., Bristow, C.S., White, K.H., 2011. Ancient watercourses and biogeography of the Sahara explain the peopling of the desert. Proc. Natl. Acad. Sci. 108, 458–462.

Drake, N.A., Breeze, P.S., Parker, A.G., 2013. Paleoclimate in the Saharan and Arabian deserts during the Middle Palaeolithic and the potential for human dispersals. Quatern. Int. 300, 48–61.

Duller, G.A.T., Tooth, S., Barham, L., Tsukamoto, S., 2015. New investigations at Kalambo Falls, Zambia: luminescence chronology, site formation, and archaeological significance. J. Hum. Evol. 85, 111–125.

Farr, L., Lane, R., Abdulazeez, F., Bennett, P., Holman, J., Marasi, A., Prendergast, A., Al-Zweyi, M., Barker, G., 2014. The Cyrenaican Prehistory Project 2013: the seventh season of excavations in the Haua Fteah cave. Libyan Studies 45, 163–173.

Fu, X., Li, B., Li, S.H., 2012. Testing a multi-step post-IR IRSL dating method using polymineral fine grains from Chinese loess. Quat. Geochronol. 10, 8–15.

Galbraith, R.F., Roberts, R.G., 2012. Statistical aspects of equivalent dose and error calculation and display in OSL dating: an overview and some recommendations. Quat. Geochronol. 11, 1–27.

Galbraith, R.F., Roberts, R.G., Laslett, G.M., Yoshida, H., Olley, J.M., 1999. Optical dating of single and multiple grains of quartz from Jinmium rock shelter, northern Australia: Part I, experimental design and statistical models. Archaeometry 41, 339–364.

Garcea, E. A.A., 2010. The spread of the Aterian peoples in North Africa. In: Garcea, E.A.A. (Ed.) South-eastern Mediterranean Peoples Between 130,000 and 10,000 Years Ago. Oxbow Books, Oxford, pp. 37–53.

Garrod, D.A.E., 1937. The Stone Age of Mount Carmel. Cambridge University Press, Cambridge.

Guérin, G., Mercier, N., Adamiec, G., 2011. Dose-rate conversion factors: update. Ancient TL 29, 5–8.

Guo, Y.J., Li, B., Zhang, J.F., Roberts, R.G., 2015. Luminescence-based chronologies for Palaeolithic sites in the Nihewan Basin, northern China: First tests using newly developed optical dating procedures for potassium feldspar grains. J. Archaeol. Sci.: Reports 3, 31–40.

Hublin, J.-J., 2000. Modern-non-modern hominid interactions: a Mediterranean perspective. In: Bar-Yosef, O., Pilbeam, D. (Eds.), The Geography of Neandertals and Modern

Humans in Europe and the Greater Mediterranean. Peabody Museum Bulletin 8, Peabody Museum of Archaeology and Ethnology, Harvard, pp. 157–182.

Huntley, D.J., Hancock, R.G.V., 2001. The Rb contents of the K-feldspars being measured in optical dating. Ancient TL 19, 43–46.

Huntley, D.J., Lamothe, M., 2001. Ubiquity of anomalous fading in K-feldspars and the measurement and correction for it in optical dating. Can. J. Earth Sci. 38, 1093–1106.

Huntley, D.J., Lian, O.B., 2006. Some observations on tunnelling of trapped electrons in feldspars and their implications for optical dating. Quaternary Sci. Rev. 25, 2503–2512.

Huntley, D.J., Godfrey-Smith, D.I., Thewalt, M.L.W., 1985. Optical dating of sediments. Nature 313, 105–107.

Inglis, R.,H., 2012. Human occupation and changing environments during the Middle to Later Stone Ages: soil micromorphology at the Haua Fteah, Libya. Ph.D. Dissertation, University of Cambridge.

Jacobs, Z., Roberts, R.G., 2007. Advances in optically stimulated luminescence dating of individual grains of quartz from archaeological deposits. Evol. Anthropol. 16, 2100–2223.

Jacobs, Z., Roberts, R.G., 2015. An improved single grain OSL chronology for the sedimentary deposits from Diepkloof Rockshelter, Western Cape, South Africa. J. Archaeol. Sci. 63, 175–192.

Jones, S.C., 2016. Middle Stone Age reduction strategies at the desert's edge: a multi-site comparison across the Gebal Akhdar of northeast Libya. Quatern. Int. 408, 53–78.

Li, B., Li, S.H., 2011. Luminescence dating of K-feldspar from sediments: a protocol without anomalous fading correction. Quat. Geochronol. 6, 468–479.

Li, B., Li, S.H., 2012. Luminescence dating of Chinese loess beyond 130 ka using the non-fading signal from K-feldspar. Quat. Geochronol. 10, 24–31.

Li, B., Jacobs, Z., Roberts, R.G., Li, S.H., 2013a. Extending the age limit of luminescence dating using the dose-dependent sensitivity of MET-pIRIR signals from K-feldspar. Quat. Geochronol. 17, 55–67.

Li, B., Roberts, R.G., Jacobs, Z., 2013b. On the dose dependency of the bleachable and non-bleachable components of IRSL from K-feldspar: improved procedures for luminescence dating of Quaternary sediments. Quat. Geochronol. 17, 1–13.

Li, B., Roberts, R.G., Jacobs, Z., Li, S.H., 2014a. A single-aliquot luminescence dating procedure for K-feldspar based on the dose-dependent MET-pIRIR signal sensitivity. Quat Geochronol 20, 51–64.

Li, B., Jacobs, Z., Roberts, R.G., Li, S.H., 2014b. Review and assessment of the potential of post-IR IRSL dating methods to circumvent the problem of anomalous fading in feldspar luminescence. Geochronometria 41, 178–201.

Li, B., Roberts, R.G., Jacobs, Z., Li, S.H., 2015a. Potential of establishing a 'global standardised growth curve' (gSGC) for optical dating of quartz from sediments. Quat. Geochronol. 27, 94–104.

Li, B., Roberts, R.G., Jacobs, Z., Li, S.H., Guo, Y.J., 2015b. Construction of a 'global standardised growth curve' (gSGC) for infrared stimulated luminescence dating of K-feldspar. Quat. Geochronol. 27, 119–130.

Li, B., Jacobs, Z., Roberts, R.G., 2016. Investigation of the applicability of standardised growth curves for OSL dating of quartz from Haua Fteah cave, Libya. Quat. Geochronol. 35, 1–15.

Lisiecki, L.E., Raymo, M.E., 2005. A Pliocene-Pleistocene stack of 57 globally distributed benthic $\delta^{18}O$ records. Paleoceanography 20, 1–17.

Lowick, S.E., Preusser, F., 2011. Investigating age underestimation in the high dose region of optically stimulated luminescence using fine grain quartz. Quat. Geochronol. 6, 33–41.

McBurney, C.B.M., 1960. The Stone Age of Northern Africa. Penguin Books, London.

McBurney, C.B.M., 1967. The Haua Fteah in Cyrenaica and the Stone Age of the South-East Mediterranean. Cambridge University Press, Cambridge.

McBurney, C.B.M., Hey, R. W., 1955. Prehistory and Pleistocene Geology in Cyrenaican Libya. Cambridge University Press, Cambridge.

Mejdahl, V., 1979. Thermoluminescence dating: beta-dose attenuation in quartz grains. Archaeometry 21, 61–72.

Nespoulet, R., El-Hajraoui, M.A., Amani, F., Ben-Ncer, A., Debenath, A., El Idrissi, A., Lacombe, J.-P., Michel, P., Oujaa, A., Stoetzel, E., 2008. Palaeolithic and Neolithic occupations in the Temara region (Rabat, Morocco): recent data on hominin contexts and behaviour. Afr. Archaeol. Rev. 25, 21–40.

Olley, J.M., Murray, A., Roberts, R.G., 1996. The effects of disequilibria in the uranium and thorium decay chains on burial dose rates in fluvial sediments. Quaternary Sci. Rev. 15, 751–760.

Olley, J.M., Roberts, R.G., Murray, A.S., 1997. Disequilibria in the uranium decay series in sedimentary deposits at Allen's Cave, Nullarbor Plain, Australia: Implications for dose rate determinations. Radiat. Meas. 27, 433–443.

Osborne, A.H., Vance, D., Rohling, E.J., Barton, N., Rogerson, M., Fello, N., 2008. A humid corridor across the Sahara for the migration of early modern humans out of Africa 120,000 years ago. Proc. Natl. Acad. Sci. 105, 16444–16447.

Prescott, J.R., Hutton, J.T., 1994. Cosmic ray contributions to dose rates for luminescence and ESR dating: large depths and long term time variations. Radiat. Meas. 23, 497–500.

Rabett, R., Farr, L., Hill, E., Hunt, C., Lane, R., Moseley, H., Stimpson, C., Barker, G., 2013. The Cyrenaican Prehistory Project 2012: the sixth season of excavations in the Haua Fteah cave. Libyan Studies 44, 113–125.

Reynolds, T.E.G., 2013. The Middle Palaeolithic of Cyrenaica: is there an Aterian at the Haua Fteah and does it matter? Quatern. Int. 300, 171–81.

Rhodes, E. J., Schwenninger, J.-L., 2007. Dose rates and radioisotope concentrations in theconcrete calibration blocks at Oxford. Ancient TL 25, 5–8.

Richter, D., Moser, J., Nami, M., Eiwanger, J., Mikdad, A., 2010. New chronometric data from Ifri n'Ammar (Morocco) and the chronostratigraphy of the Middle Palaeolithic in the Western Maghreb. J. Hum. Evol. 59, 672–679.

Roberts, H.M., Duller, G.A.T., 2004. Standardised growth curves for optical dating of sediment using multiple-grain aliquots. Radiat. Meas. 38, 241–252.

Roberts, R.G., Jacobs, Z., Li, B., Jankowski, N.R., Cunningham, A.C., Rosenfeld, A.B., 2015. Optical dating in archaeology: thirty years in retrospect and grand challenges for the future. J. Archaeol. Sci. 56, 41–60.

Rust, A., 1950. Die Höhlenfunde von Jabrud, Syrien. Wacholtz, Neumünster.

Russell, N., Armitage, S., 2012. A comparison of single-grain and small aliquot dating of fine sand from Cyrenaica, northern Libya. Quat. Geochronol. 10, 62–67.

Sanchez-Goñi, M.F., Harrisson, S.P., 2010. Millennial-scale climate variability and vegetation changes during the Last Glacial: concepts and terminology. Quaternary Sci. Rev. 29, 2823–2827.

Scerri, E., 2013. The Aterian and its place in the North African Middle Stone Age. Quatern. Int. 300, 111–130.

Schild, R., Wendorf, F., 1993. Middle Paleolithic lakes in the southwestern desert of Egypt. In: Wendorf, F., Schild, R., Close, A.E. (Eds.), Egypt During the Last Interglacial. The Middle Paleolithic of Bir Tarfawi and Bir Sahara East. Plenum Press, New York, pp. 15–65.

Smedley, R.K., Duller, G.A.T., Pearce, N.J.G., Roberts, H.M., 2012. Determining the K-content of single-grains of feldspar for luminescence dating. Radiat. Meas. 47, 790–796.

Smith, M.A., Prescott, J.R., Head, M.J., 1997. Comparison of ^{14}C and luminescence chronologies at Puritjarra rock shelter, central Australia. Quaternary Sci. Rev. 16, 299–320.

Sohbati, R., Murray, A.S., Buylaert, J.P., Ortuno, M., Cunha, P.P., Masana, E., 2012. Luminescence dating of Pleistocene alluvial sediments affected by the Alhama de

Murcia fault (eastern Betics, Spain) – a comparison between OSL, IRSL and post-IR IRSL ages. Boreas 41, 250–262.

Spooner, N.A., 1992. Optical dating: preliminary results on the anomalous fading of luminescence from feldspars. Quaternary Sci. Rev. 11, 139–145.

Spooner, N.A., 1994. The anomalous fading of infrared-stimulated luminescence from feldspars. Radiat. Meas. 23, 625–632.

Thiel, C., Buylaert, J.P., Murray, A., Terhorst, B., Hofer, I., Tsukamoto, S., Frechen, M., 2011. Luminescence dating of the Stratzing loess profile (Austria) – testing the potential of an elevated temperature post-IR IRSL protocol. Quatern. Int. 234, 23–31.

Thomsen, K.J., Murray, A.S., Jain, M., Bøtter-Jensen, L., 2008. Laboratory fading rates of various luminescence signals from feldspar-rich sediment extracts. Radiat. Meas. 43, 1474–1486.

Trinkaus, E., 2005. Early modern humans. A. Rev. Anthropol. 34, 207–230.

Van Peer, P., 1991 Inter-assemblage variability and Levallois styles: the case of the Northern African Middle Palaeolithic. J. Anthropol. Archaeol. 10, 107–151.

Van Peer, P., Vermeersch, P.M., 2007. The place of northeast Africa in the early history of modern humans: new data and interpretations on the Middle Stone Age. In: Mellars, P., Boyle, K., Bar-Yosef, O., Stringer, C. (Eds.), Rethinking the Human Revolution: New Behavioural and Biological Perspectives on the Origin and Dispersal of Modern Humans. Cambridge, McDonald Institute for Archaeological Research Monographs, Cambridge, pp. 187–198.

Vermeersch, P.M., 2010. Middle and Upper Palaeolithic in the Egyptian Nile Valley. In: Garcea, E.A.A. (Ed.), South-Eastern Mediterranean Peoples Between 130,000 and 10,000 Years Ago. Oxbow Books, Oxbow, pp. 66–88.

Wintle, A.G., 1973. Anomalous fading of thermoluminescence in mineral samples. Nature 245, 143–144.

Wintle, A.G., 2014. Luminescence dating methods. In: Holland, H., Turekian, K. (Eds.), Treatise on Geochemistry, second ed., vol. 14. Elsevier, Oxford, pp. 17–35.

Wrinn, P.J., Rink, W.J., 2003. Complete ESR dating of tooth enamel from Aterian levels at Mugharet el' Aliya (Tangier, Morocco). J. Archaeol. Sci. 30, 123–133.

Captions to the figures and tables

Figure 1. The Haua Fteah cave (Cyrenaica, northeast Libya), showing (a) its location in northeast Libya, (b) the entrance to the cave, (c) the 1950s McBurney excavations, and (d) schematic diagram of the stepped McBurney trench and the TRANS-NAP trenches down its sides (U, M, D and S). (b: photograph by Graeme Barker; c: reproduced with the permission of the Museum of Archaeology and Anthropology, University of Cambridge; a, d: illustrations by Lucy Farr.)

Figure 2. The McBurney trench emptied of backfill: (a) Upper and Middle Trenches, with TRANS-NAP Trench M visible cut into the north-facing face of the Middle Trench; (b) Middle Trench and Deep Sounding, showing the TRANS-NAP Trenches M and (below it) D under excavation. (Photographs: Graeme Barker.)

Figure 3. Modelled ages for the sedimentary facies and McBurney cultural phases in the Upper and Middle Trenches proposed by Douka et al. (2014).

Figure 4. The south-facing section of the Deep Sounding, and Trench S below it, showing the stratigraphic units defined by the present project and the locations of the samples taken for optical dating. (Drawing: Lucy Farr, based on field drawings by Ross Lane, Alex Pryor, Ryan Rabett, Hazel Mosely and Hazel Reade.)

Figure 5. Trench S at the end of excavation, showing the accumulation of sharp-edged rocks likely from a substantial rock fall from the cave roof, with fine red silts in between them. Looking east. Vertical scale: 20 cm divisions; horizontal scale: 10 cm divisions. (Photograph: Graeme Barker.)

Figure 6. Burrows in the soft sediments of Trench D, assumed to be of mole-rats, viewed from the north: one crosses the trench diagonally on the left, and one is clearly visible vertically up the image to the right-hand end of the 1 m ranging pole. (Photograph: Graeme Barker.)

Figure 7. (a) Typical dose response curves for three aliquots of sample HF11. The data sets for aliquots #1 and #2 were fitted using a single saturating exponential function $Y = A[1–\exp(–X/D_0)]+Y_0$, where Y is the test dose-corrected signal, X is the regenerative dose, D_0 is the characteristic saturation dose, and A and Y_0 are constants. The data for aliquot #3 were fitted using a single saturating exponential function plus an extra linear term $Y = A[1–\exp(–X/D_0)]+CX+Y_0$, where C is a constant. (b) The central age model estimates of the re-normalized signals for the three groups of aliquots at each regenerative dose for samples HF1, HF3, HF10 and HF11.

Figure 8. Representative IRSL (50°C) and MET-pIRIR (100–250°C) decay curves for a natural aliquot (of sample HF6021) stimulated at the temperature shown above each curve.

Figure 9. Re-normalized dose response curves for the MET-pIRIR signals measured at different temperatures for samples HF6019, HF6021 and HF6023. The L_x/T_x and L_x data are shown in the left– and right–hand panels, respectively. The data points in each of the figures

were fitted using a single saturating exponential function (dashed lines). For comparison, the solid line in panels a, c, e and g is the best-fit curve for the 250°C L_x/T_x signal, (shown as the dashed line in panel i).

Figure 10. Comparison of the D_e values obtained using single aliquot SGCs and individual SAR curves for the 250 °C L_x/T_x (a) and L_x (c) signals. The ratios between them are shown in the radial plots (b) and (d), respectively.

Figure 11. Residual doses measured for the 250 °C L_x/T_x signal for nine samples, plotted against their corresponding D_e values. The data set was fitted using a linear regression (solid line) to calculate and intercept on the y-axis of 3.1 ± 1.3 Gy.

Figure 12. Ratios of measured-dose to given dose, plotted as a function of infrared stimulation temperature for samples HF6019, HF6021 and HF6043; the given doses are indicated in each plot. The solid lines demarcate ratios of 0.9 and 1.1, and the dashed line represents a ratio of unity.

Figure 13. Anomalous fading rate (g-value) of the L_x/T_x MET-pIRIR signal plotted against infrared stimulation temperature for sample HF6021.

Figure 14. D_e values plotted against infrared stimulation temperature for each of the samples dated in this study. The filled circles and open squares represent values obtained for the L_x/T_x signal and L_x signal, respectively. For samples HF4, HF8, HF10 and HF11, results were obtained only for the L_x/T_x signal, for comparison with quartz OSL ages (see text).

Figure 15. Changing frequencies of lithic material (McBurney finds) in the Deep Sounding of the Haua Fteah: number of complete blanks (x axis) and total weights (in grams) of struck lithics (complete blanks, broken blanks, cores, core fragments and flaked pieces) recovered from each excavated spit of the Deep Sounding (y axis). (Analysis: Sacha Jones.)

Figure 16. Optical ages for the Haua Fteah plotted against the LR04 Marine Isotope Stage chronology and stacked benthic oxygen isotope curve (Lisiecki and Raymo, 2005). Ages are plotted with 1σ errors in schematic stratigraphic order. (Drawing: Lucy Farr.)

Table 1. Summary of SAR and SGC quartz OSL ages for each group (‘early’, ‘medium’ and later’) determined from the D_e values of six samples reported in Li et al. (2016) and the single aliquot and single grain OSL ages presented in Douka et al. (2014).

Table 2. The MET-pIRIR and pre-dose MET-pIRIR procedures used to measure K-feldspars in this study.

Table 3. Summary of sample burial depths, contexts, dose rate information, equivalent dose (D_e) values and MET-pIRIR age estimates for K-feldspar grains. The four samples from the Middle Trench (HF4, HF8, HF10 and HF11) were dated using the MET-pIRIR signal. The other samples from the Deep Sounding (HF6012–6045) and Trench S (HF6008 and 6009) were dated using the pMET-pIRIR signals**.**

Table 1:

Sample	Method	Age (ka) – this study[a]			Age (ka) – Douka et al. (2014)	
		Early	Medium	Later	Single aliquot	Single grain
HF1	SAR	18.9 ± 1.1	18.4 ± 1.0	17.5 ± 1.0	18.9 ± 1.0	19.3 ± 1.4
	SGC	17.0 ± 1.0	18.3 ± 1.1	18.3 ± 1.1		
HF3	SAR	31.5 ± 2.8	32.6 ± 2.8	32.7 ± 2.8	32.4 ± 2.8	31.9 ± 3.5
	SGC	30.9 ± 2.7	33.0 ± 2.9	33.6 ± 2.9		
HF4	SAR	*30.8 ± 3.3*	39.9 ± 3.8	**37.2 ± 3.7**	38.2 ± 3.7	—
	SGC	*27.3 ± 2.7*	41.3 ± 4.1	36.9 ± 3.8		
HF8	SAR	*38.3 ± 4.9*	49.0 ± 4.6	**50.1 ± 4.9**	49.8 ± 4.7	46.2 ± 4.5
	SGC	*29.7 ± 3.2*	51.7 ± 5.0	51.6 ± 5.0		
HF10	SAR	*51.8 ± 5.5*	62.2 ± 6.4	**65.8 ± 6.8**	60.9 ± 6.1	63.7 ± 6.6
	SGC	*32.3 ± 3.4*	63.8 ± 6.5	65.4 ± 6.8		
HF11	SAR	*56.6 ± 6.3*	70.0 ± 6.5	**70.0 ± 6.7**	65.8 ± 6.0	70.9 ± 7.0
	SGC	*44.8 ± 4.3*	74.2 ± 6.8	71.2 ± 6.7		

[a] Ages determined from the D_e values presented in Li et al. (2016) and the dose rates presented in Douka et al. (2014). Ages in italics represent underestimations of the true sample mean age because their D_e values were calculated from a truncated D_e distribution. Ages in bold and shaded grey are considered the most reliable ages for these samples as these are not affected by saturation issues within the range of doses relevant to D_e estimation.

Table 2:

Step	(a) MET-pIRIR	(b) Pre-dose MET-pIRIR	Observed
1	Give regenerative dose, D_i [a]	Give regenerative dose, D_i [a]	
2	Preheat at 300 °C for 60 s	Preheat at 300 °C for 60 s	
3	IRSL measurement at 50 °C for 100 s	IRSL measurement at 50 °C for 100 s	$L_{x(50)}$
4	IRSL measurement at 100 °C for 100 s	IRSL measurement at 100 °C for 100 s	$L_{x(100)}$
5	IRSL measurement at 150 °C for 100 s	IRSL measurement at 150 °C for 100 s	$L_{x(150)}$
6	IRSL measurement at 200 °C for 100 s	IRSL measurement at 200 °C for 100 s	$L_{x(200)}$
7	IRSL measurement at 250 °C for 100 s	IRSL measurement at 250 °C for 100 s	$L_{x(250)}$
8	Give test dose, D_t	Give test dose, D_t	
9	Preheat at 300 °C for 60 s	Preheat at 300 °C for 60 s	
10	IRSL measurement at 50 °C for 100 s	IRSL measurement at 50 °C for 100 s	$T_{x(50)}$
11	IRSL measurement at 100 °C for 100 s	IRSL measurement at 100 °C for 100 s	$T_{x(100)}$
12	IRSL measurement at 150 °C for 100 s	IRSL measurement at 150 °C for 100 s	$T_{x(150)}$
13	IRSL measurement at 200 °C for 100 s	IRSL measurement at 200 °C for 100 s	$T_{x(200)}$
14	IRSL measurement at 250 °C for 100 s	IRSL measurement at 250 °C for 100 s	$T_{x(250)}$
15	IR bleach at 320 °C for 100 s	Solar simulator bleach, 2 hr	
17	Return to step 1	Return to step 1	

[a] For the natural sample, $D_i = 0$ and the observed signals are L_n and T_n. The entire sequence is repeated for several regenerative doses and includes a zero dose and a repeat dose.

Table 3:

Sample code	Depth[a] (cm)	Sample context	Grain diameter (μm)	Field water content (%)	External dose rate (Gy/ka)			Internal dose rate (Gy/ka)	Total dose rate (Gy/ka)	D_e (Gy)[b]	Age (ka)[c]
					Gamma	Beta	Cosmic				
HF4	220	235,439, 444,453	90–125	30.7 ± 4.6	0.71 ± 0.04	1.78 ± 0.13	0.042	0.39 ± 0.09	2.92 ± 0.16	97 ± 5	33.2 ± 2.6
HF8	415	513	180–212	29.2 ± 4.4	0.70 ± 0.04	1.30 ± 0.10	0.039	0.67 ± 0.15	2.70 ± 0.18	146 ± 5	54.0 ± 4.2
HF10	460	524	125–180	34.6 ± 5.2	0.72 ± 0.04	1.28 ± 0.10	0.038	0.53 ± 0.13	2.57 ± 0.17	183 ± 9	71.2 ± 5.8
HF11	480	528	90–125	28.4 ± 4.3	0.72 ± 0.04	1.12 ± 0.08	0.037	0.39 ± 0.09	2.27 ± 0.13	165 ± 7	72.8 ± 5.2
HF6035	570	770	90–180	30.0 ± 4.6	0.71 ± 0.05	1.47 ± 0.08	0.025	0.48 ± 0.13	2.69 ± 0.16	279 ± 11	103.8 ± 7.4
HF6045	590	776	90–150	23.0 ± 3.4	0.76 ± 0.05	1.82 ± 0.09	0.025	0.43 ± 0.11	3.01 ± 0.15	269 ± 9	89.5 ± 5.3
HF6031	675	798	150–180	26.2 ± 3.9	0.60 ± 0.04	1.22 ± 0.06	0.025	0.57 ± 0.13	2.40 ± 0.15	245 ± 14	102.2 ± 8.7
HF6029	745	811	90–150	29.0 ± 4.4	0.80 ± 0.06	1.74 ± 0.09	0.025	0.43 ± 0.11	2.98 ± 0.15	355 ± 12	119.1 ± 7.2
HF6027	795	817	90–150	33.7 ± 5.1	0.76 ± 0.06	1.60 ± 0.09	0.025	0.43 ± 0.11	2.80 ± 0.15	355 ± 17	126.7 ± 9.1
HF6025	840	824	90–180	17.5 ± 3.5	0.91 ± 0.06	1.80 ± 0.09	0.023	0.48 ± 0.13	3.19 ± 0.17	380 ± 21	119.1 ± 9.1
HF6012	845	828	90–180	21.9 ± 4.4	0.89 ± 0.05	1.74 ± 0.10	0.022	0.48 ± 0.13	3.11 ± 0.17	377 ± 12	121.4 ± 7.6
HF6023	850	825	180–212	23.1 ± 4.6	0.87 ± 0.07	1.59 ± 0.09	0.022	0.67 ± 0.15	3.15 ± 0.19	395 ± 21	125.5 ± 10.1
HF6021	870	827	180–212	26.1 ± 5.2	0.92 ± 0.07	1.66 ± 0.10	0.020	0.67 ± 0.15	3.26 ± 0.20	416 ± 11	127.4 ± 8.4
HF6043	910	832	90–125	21.0 ± 4.2	1.02 ± 0.07	2.01 ± 0.11	0.020	0.39 ± 0.09	3.44 ± 0.16	468 ± 26	135.8 ± 9.8
HF6019	910	832	180–212	21.0 ± 4.2	1.02 ± 0.07	1.90 ± 0.11	0.020	0.67 ± 0.15	3.63 ± 0.19	463 ± 32	127.4 ± 11.1
HF6017	990	837	150–180	24.0 ± 4.8	0.73 ± 0.06	1.90 ± 0.11	0.020	0.57 ± 0.13	3.18 ± 0.18	474 ± 16	149.1 ± 9.8
HF6009[d]	35	752	150–180	22.6 ± 4.5	0.77 ± 0.06	1.97 ± 0.11	0.018	0.57 ± 0.13	3.29 ± 0.18	493 ± 20	150.0 ± 10.2
HF6008[d]	75	752	150–180	21.9 ± 4.4	0.76 ± 0.06	1.98 ± 0.11	0.015	0.57 ± 0.13	3.28 ± 0.18	503 ± 19	153.3 ± 10.1

[a] Approximate depths below the upper surface of the Middle Trench. Depths for HF6009 and HF6008 are below the base of the Deep Sounding.

[b] A residual dose of 3.1 ± 1.3 Gy was subtracted from each of the De values and the error added in quadrature.

[c] Mean ± standard error (1σ). A relative error of 2% was included in the uncertainty on the final ages to allow for possible bias in the calibration of the laboratory beta source.

[d] Samples collected from Trench S. All other samples were collected from the cleaned section walls of McBurney's original excavations.

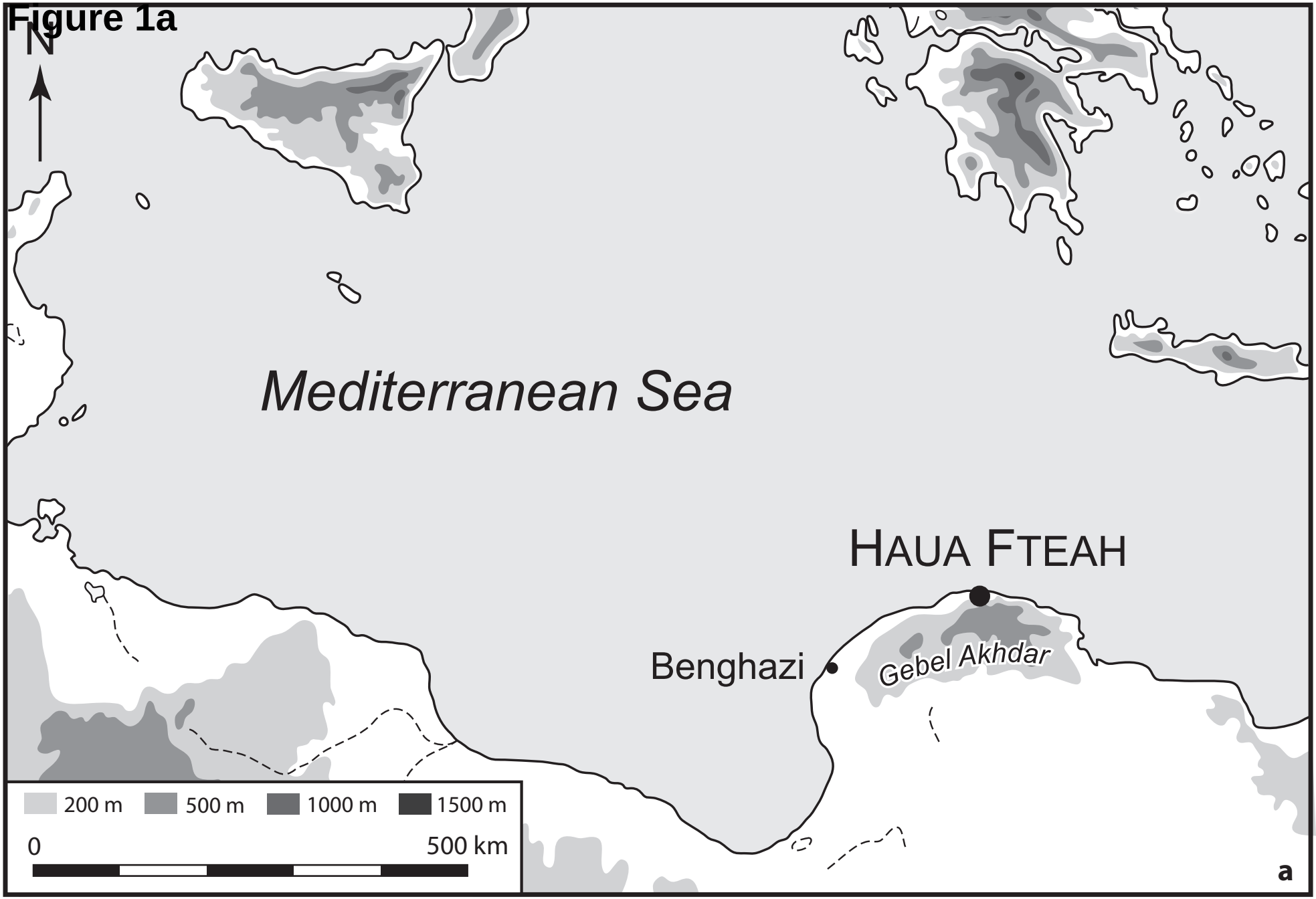
Figure 1a
N
Mediterranean Sea
HAUA FTEAH
Benghazi
Gebel Akhdar
200 m
500 m
1000 m
1500 m
0
500 km
a

Figure 1b

Click here to download high resolution image

Figure 1c

Click here to download high resolution image

Figure 1d

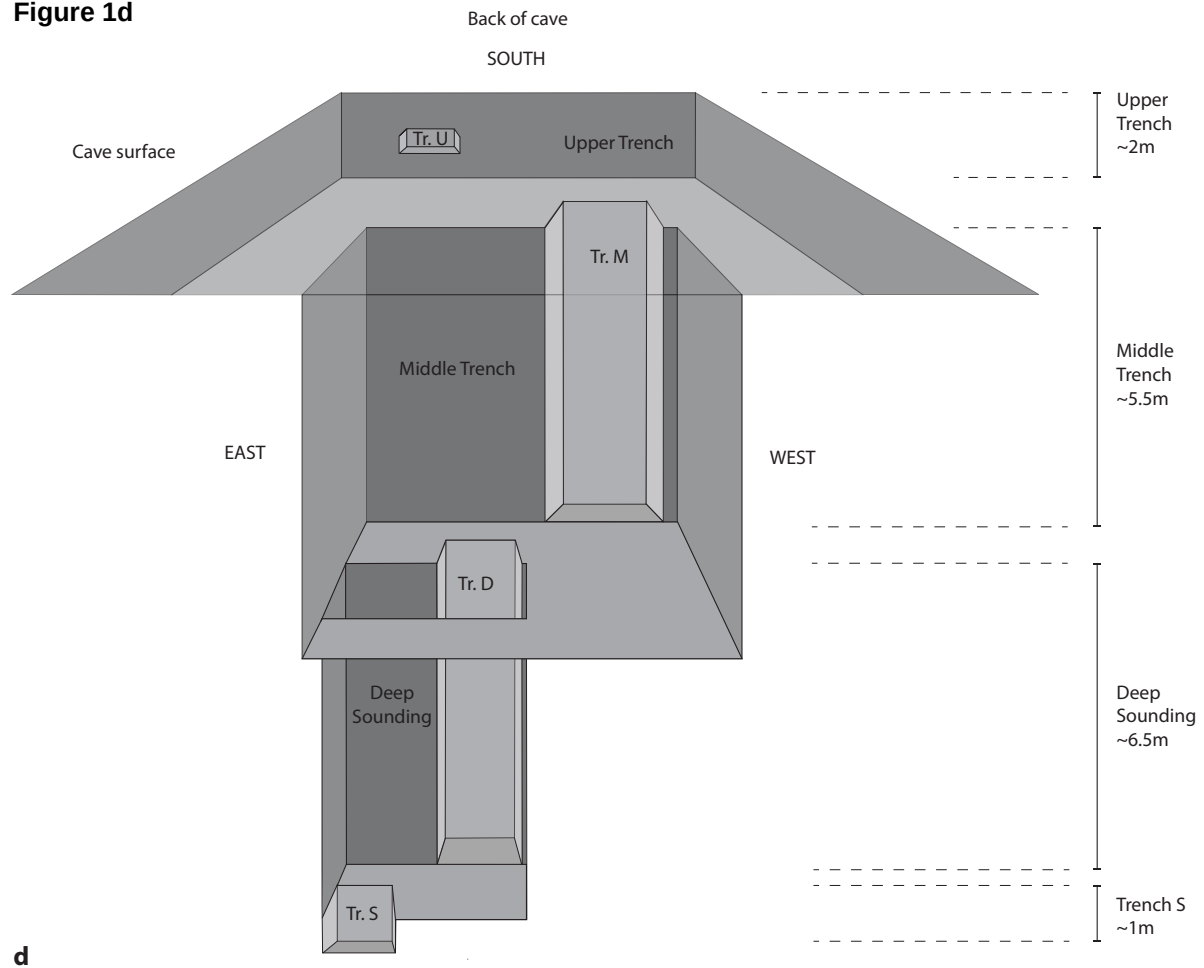
Back of cave
SOUTH
Cave surface
Tr. U
Upper Trench
Tr. M
Middle Trench
EAST
WEST
Tr. D
Deep Sounding
Tr. S
Upper Trench ~2m
Middle Trench ~5.5m
Deep Sounding ~6.5m
Trench S ~1m

d

Figure 2a
Click here to download high resolution image

Figure 2b

Click here to download high resolution image

Figure 3

Click here to download high resolution image

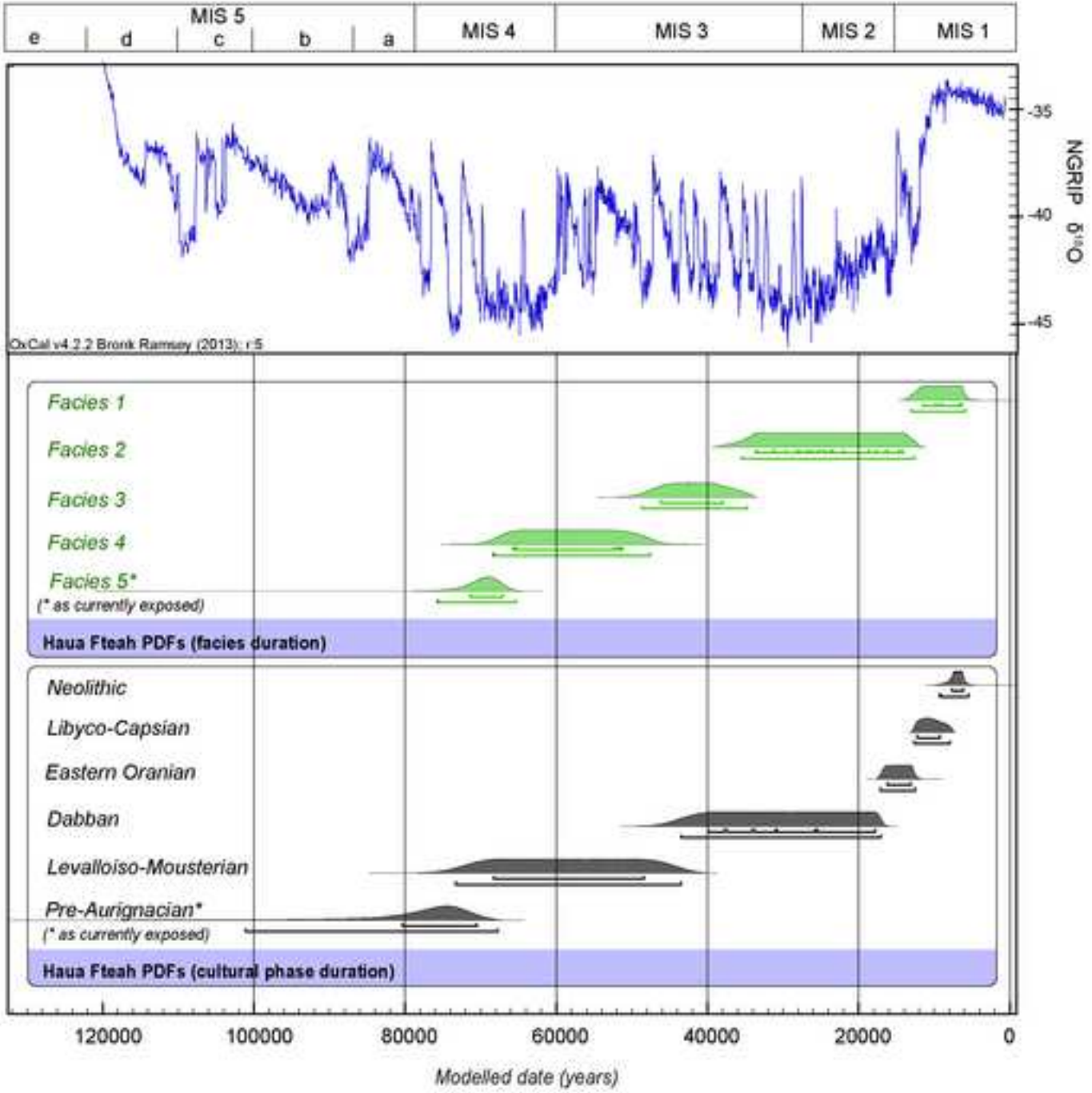

Figure 4

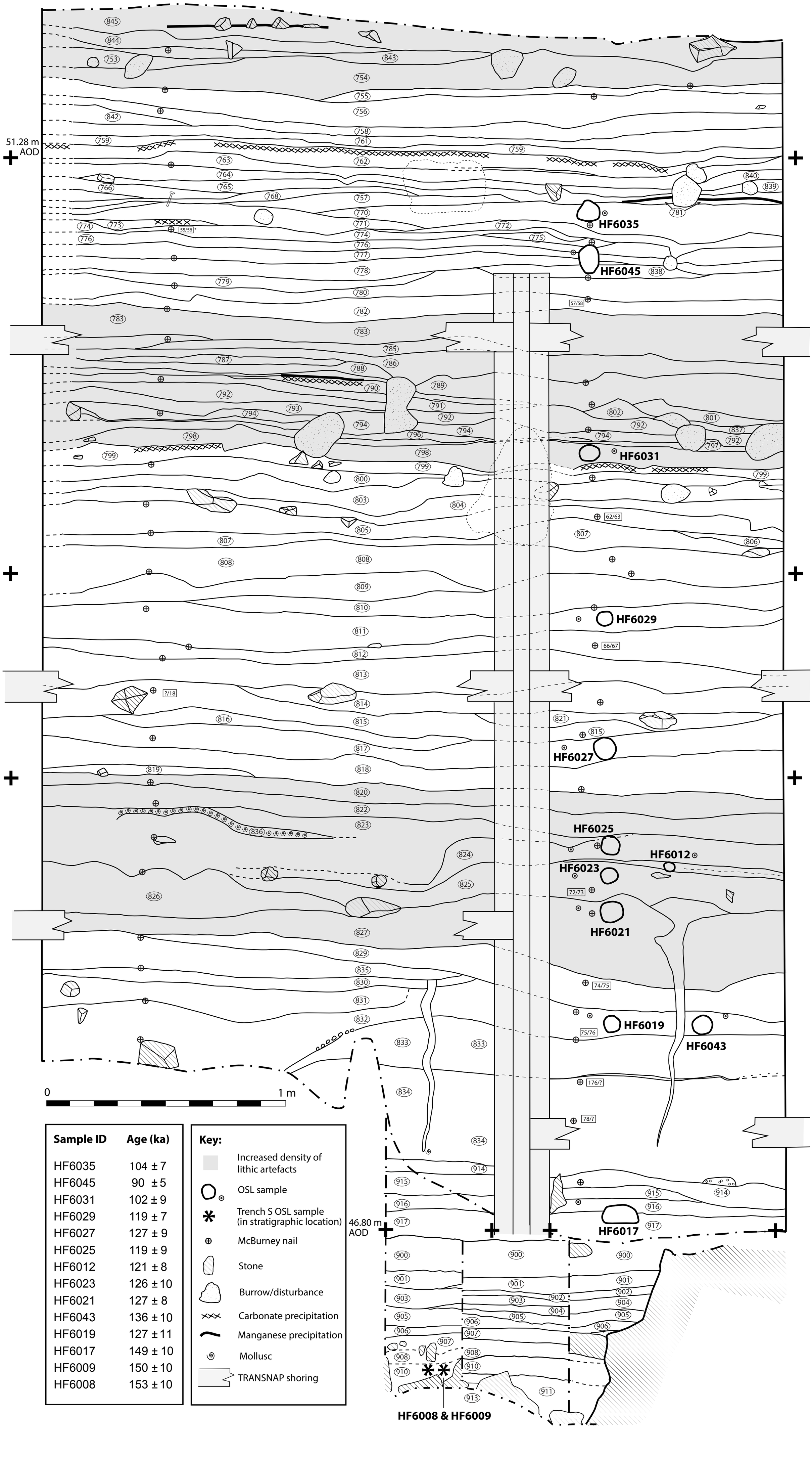

Sample ID	Age (ka)
HF6035	104 ± 7
HF6045	90 ± 5
HF6031	102 ± 9
HF6029	119 ± 7
HF6027	127 ± 9
HF6025	119 ± 9
HF6012	121 ± 8
HF6023	126 ± 10
HF6021	127 ± 8
HF6043	136 ± 10
HF6019	127 ± 11
HF6017	149 ± 10
HF6009	150 ± 10
HF6008	153 ± 10

Key:

- Increased density of lithic artefacts
- OSL sample
- Trench S OSL sample (in stratigraphic location)
- McBurney nail
- Stone
- Burrow/disturbance
- Carbonate precipitation
- Manganese precipitation
- Mollusc
- TRANSNAP shoring

Figure 5

Click here to download high resolution image

Figure 6

Click here to download high resolution image

Figure 7

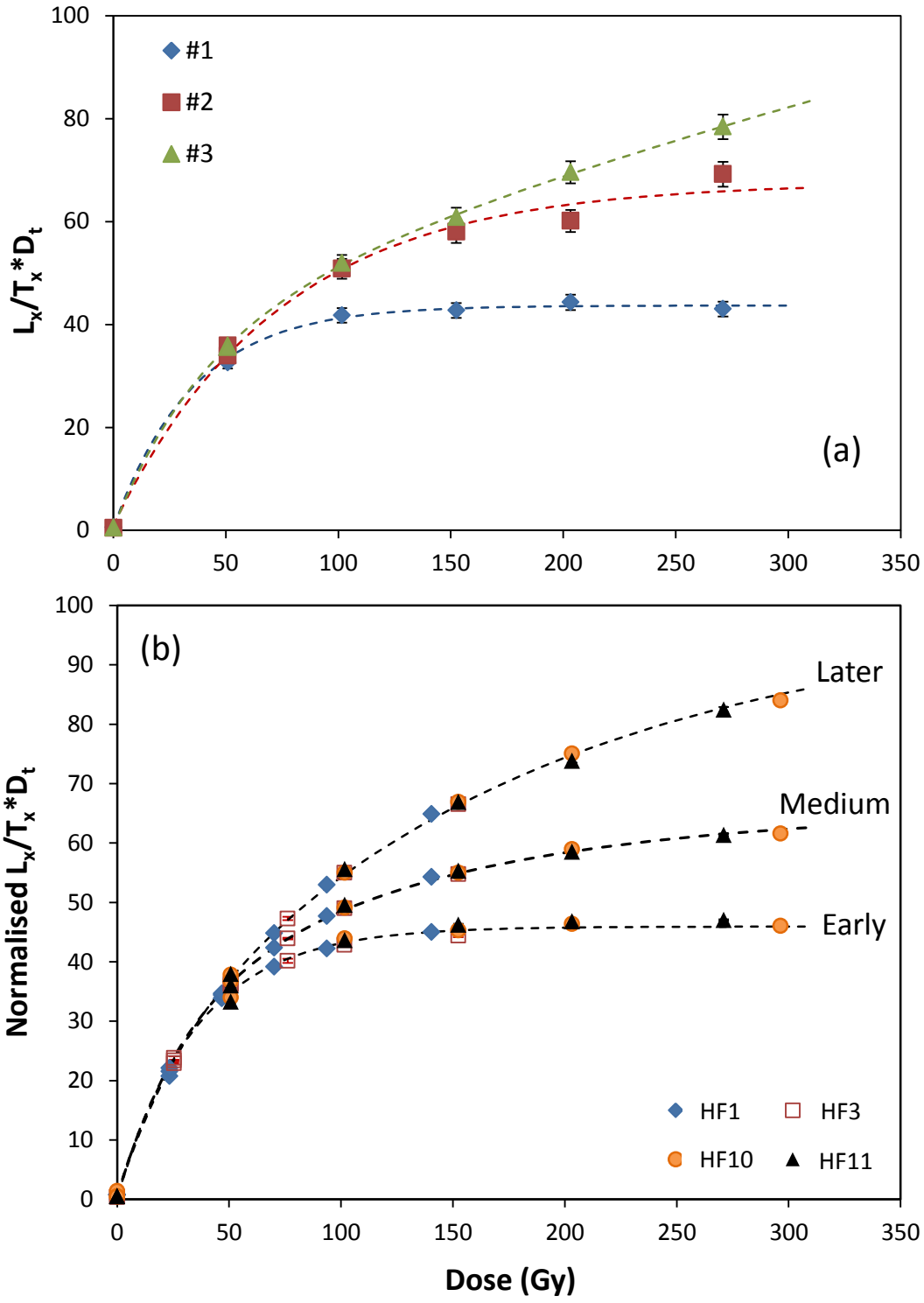

Figure 7:

Figure 8

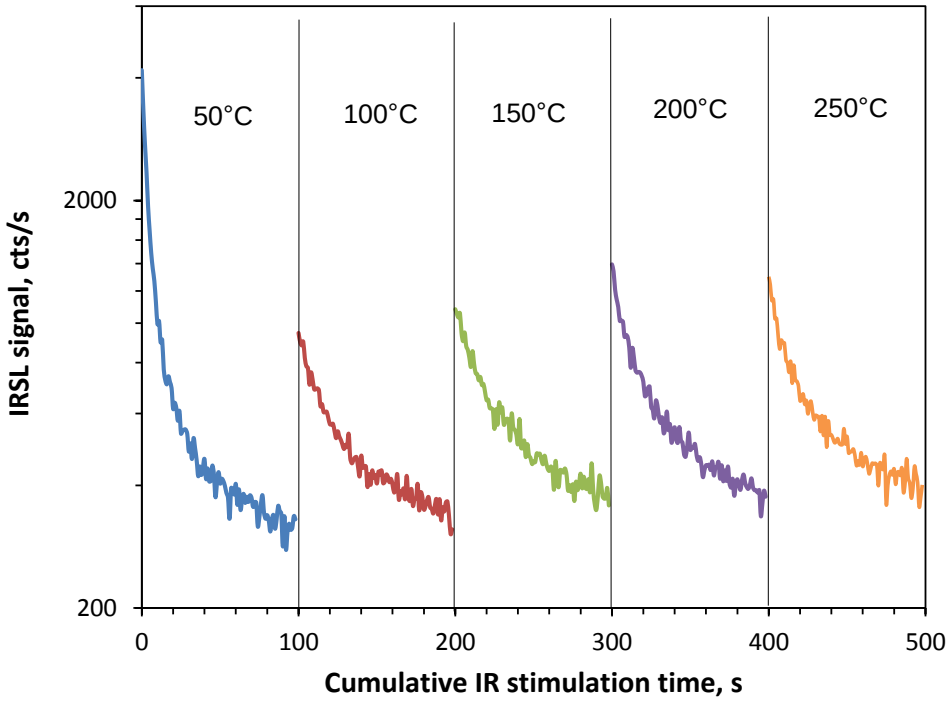

Figure 8:

Figure 9

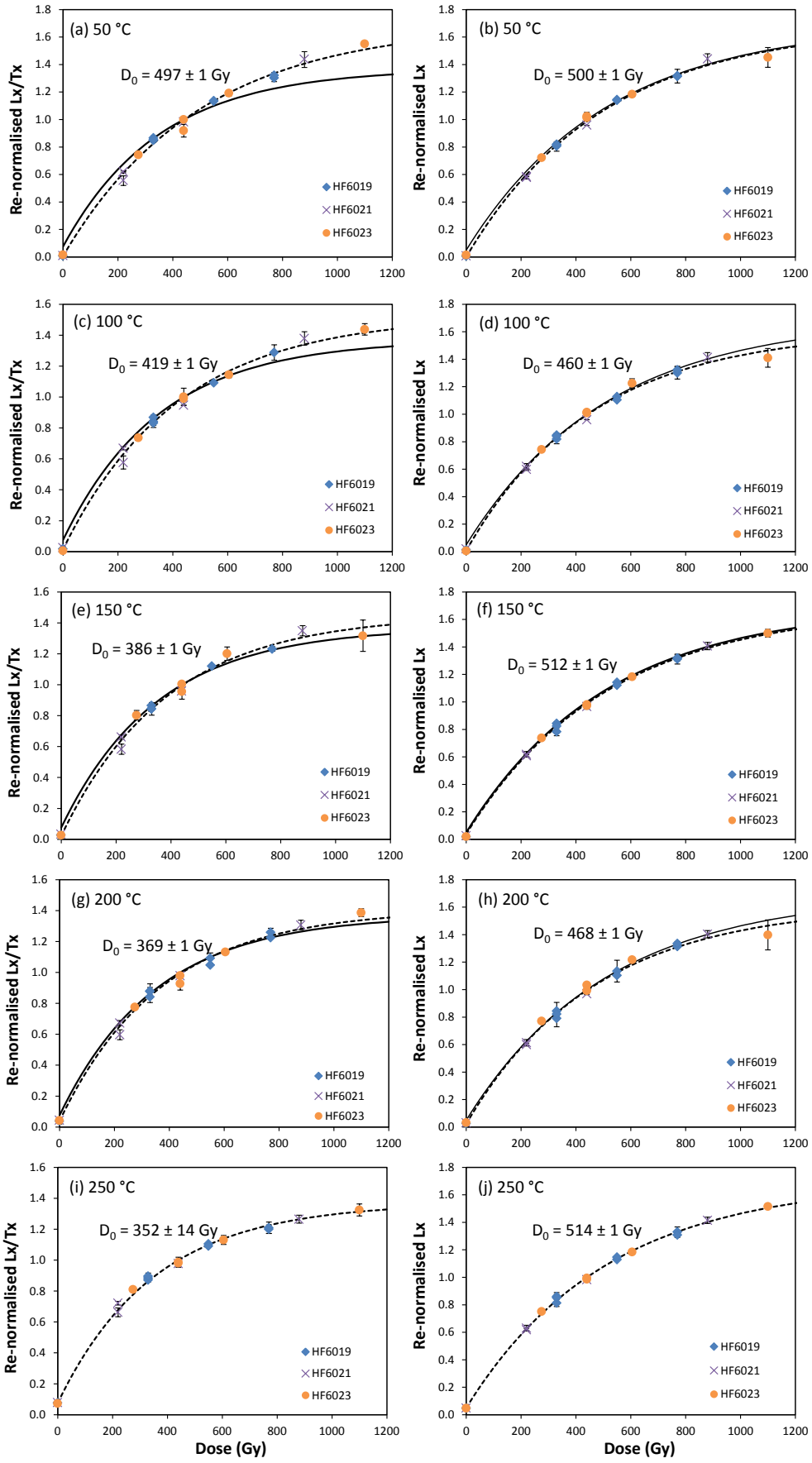
(a) 50 °C
D0 = 497 ± 1 Gy
(b) 50 °C
D0 = 500 ± 1 Gy
(c) 100 °C
D0 = 419 ± 1 Gy
(d) 100 °C
D0 = 460 ± 1 Gy
(e) 150 °C
D0 = 386 ± 1 Gy
(f) 150 °C
D0 = 512 ± 1 Gy
(g) 200 °C
D0 = 369 ± 1 Gy
(h) 200 °C
D0 = 468 ± 1 Gy
(i) 250 °C
D0 = 352 ± 14 Gy
(j) 250 °C
D0 = 514 ± 1 Gy
Re-normalised Lx/Tx
Re-normalised Lx
Dose (Gy)
HF6019
HF6021
HF6023

Figure 10

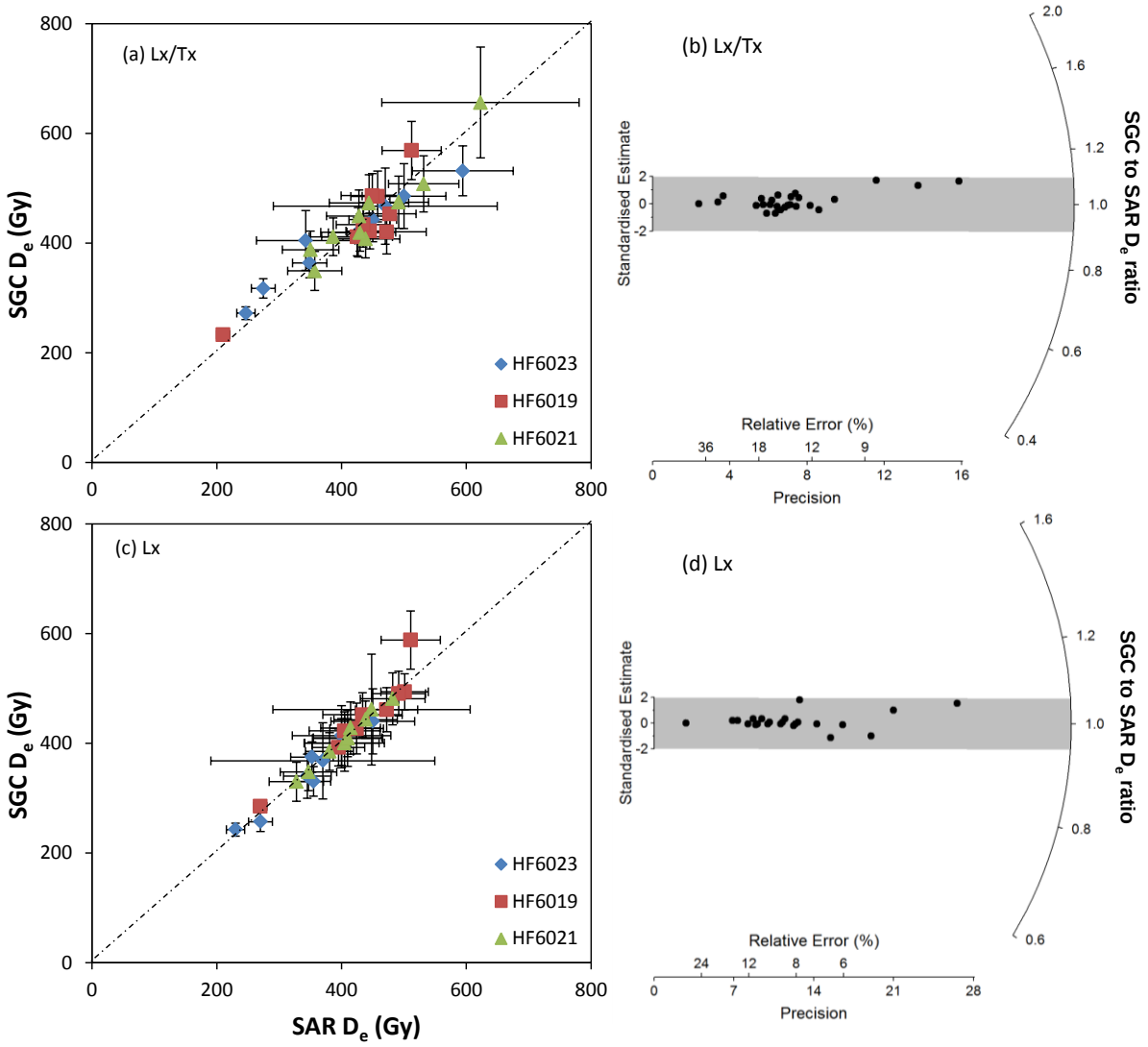

Figure 10:

Figure 11

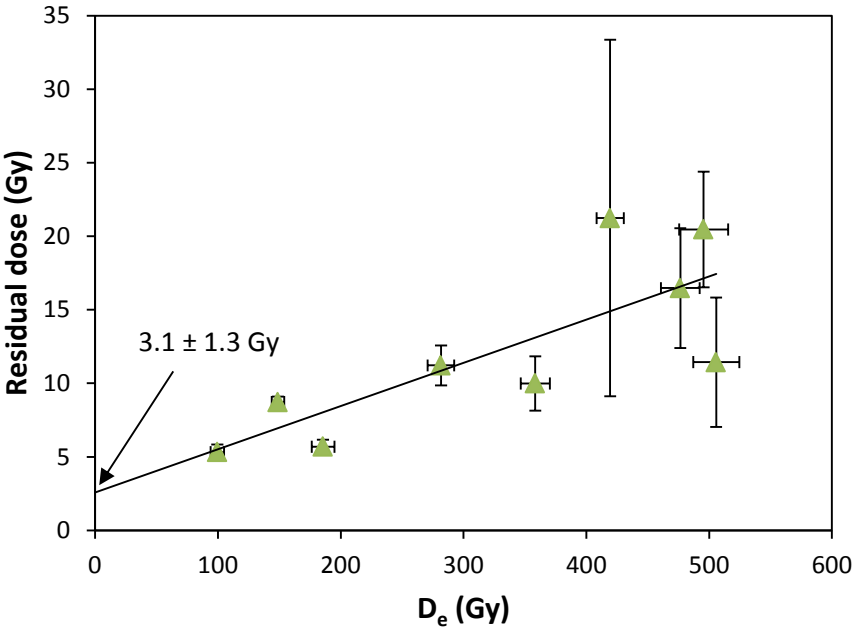

Figure 11:

Figure 12

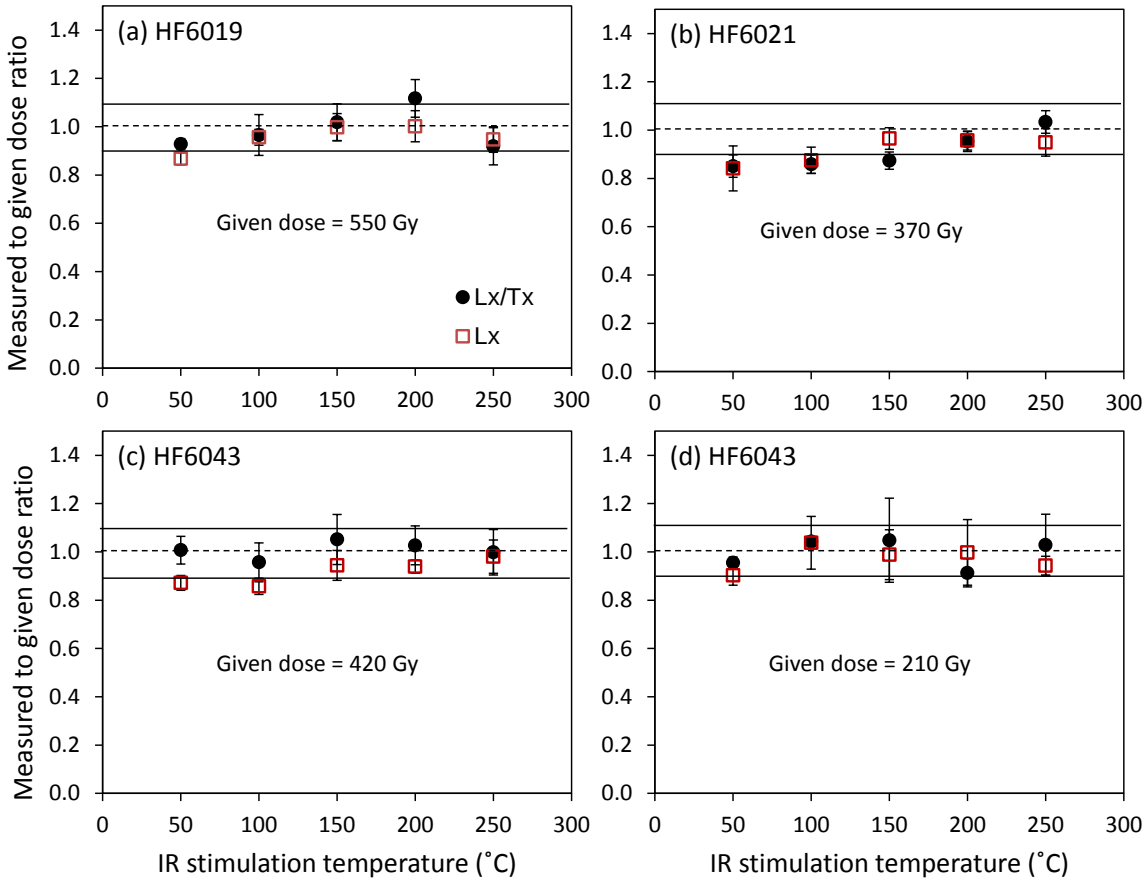

Figure 12:

Figure 13

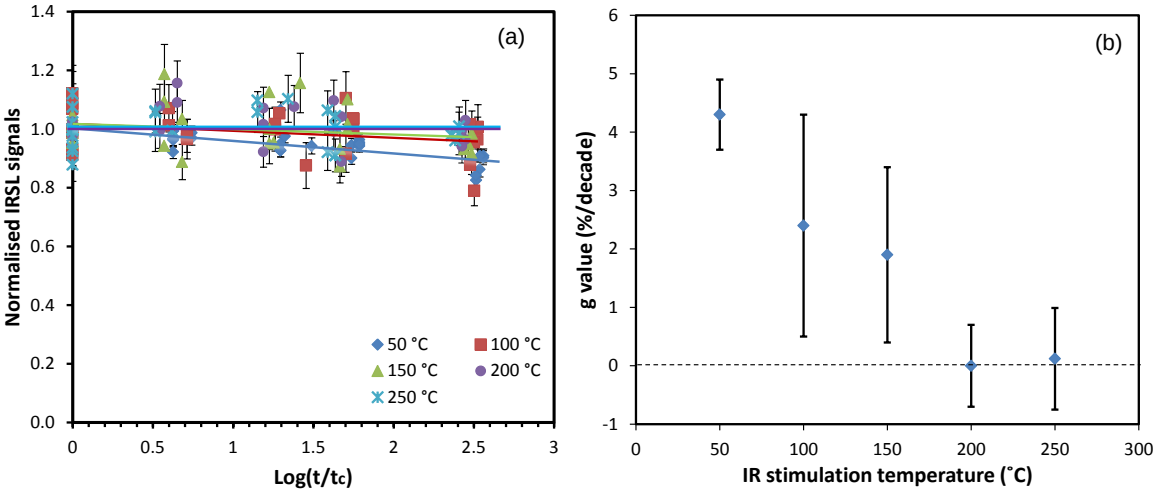

Figure 13:

Figure 14

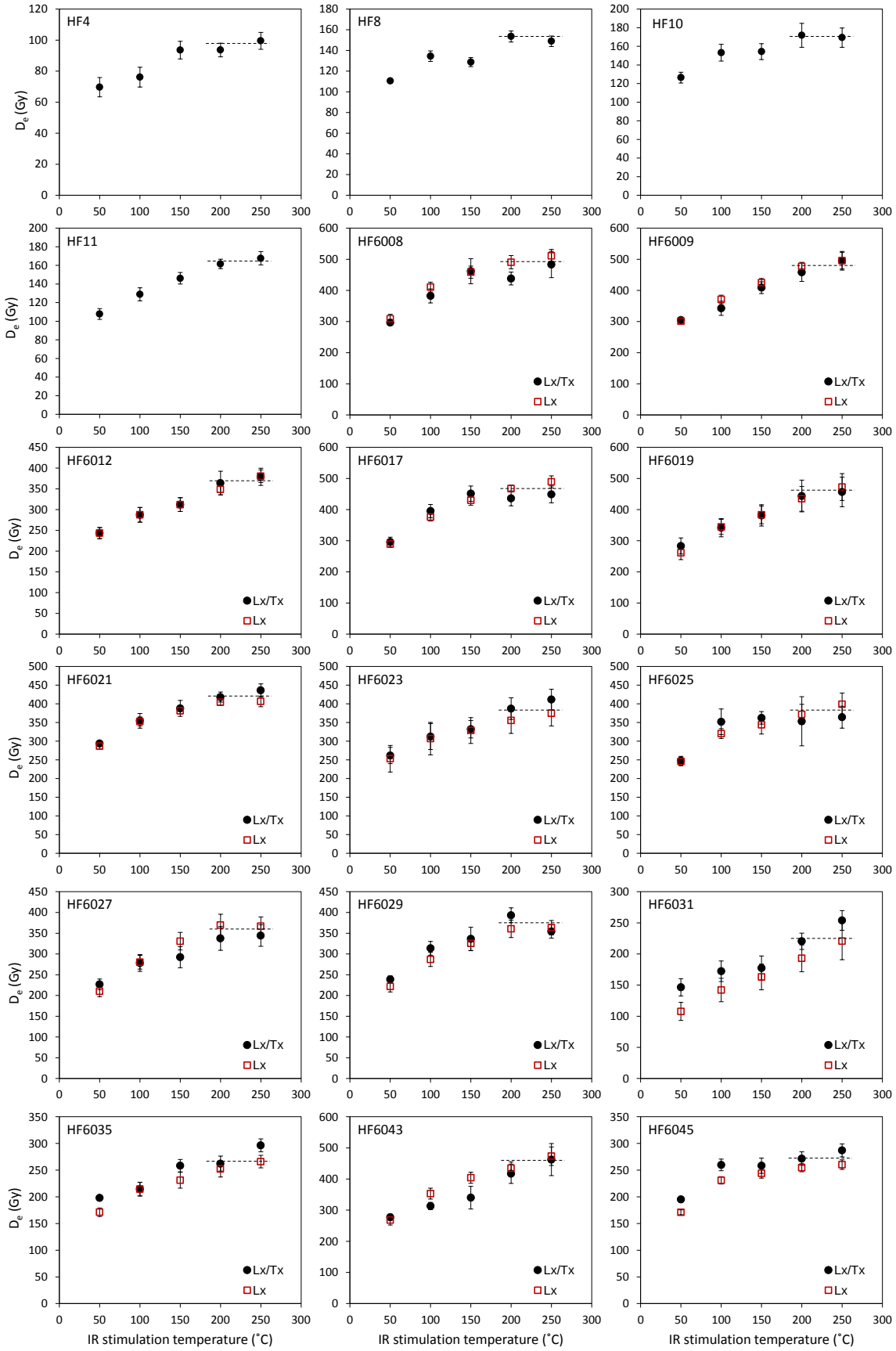

Figure 14:

Figure 15

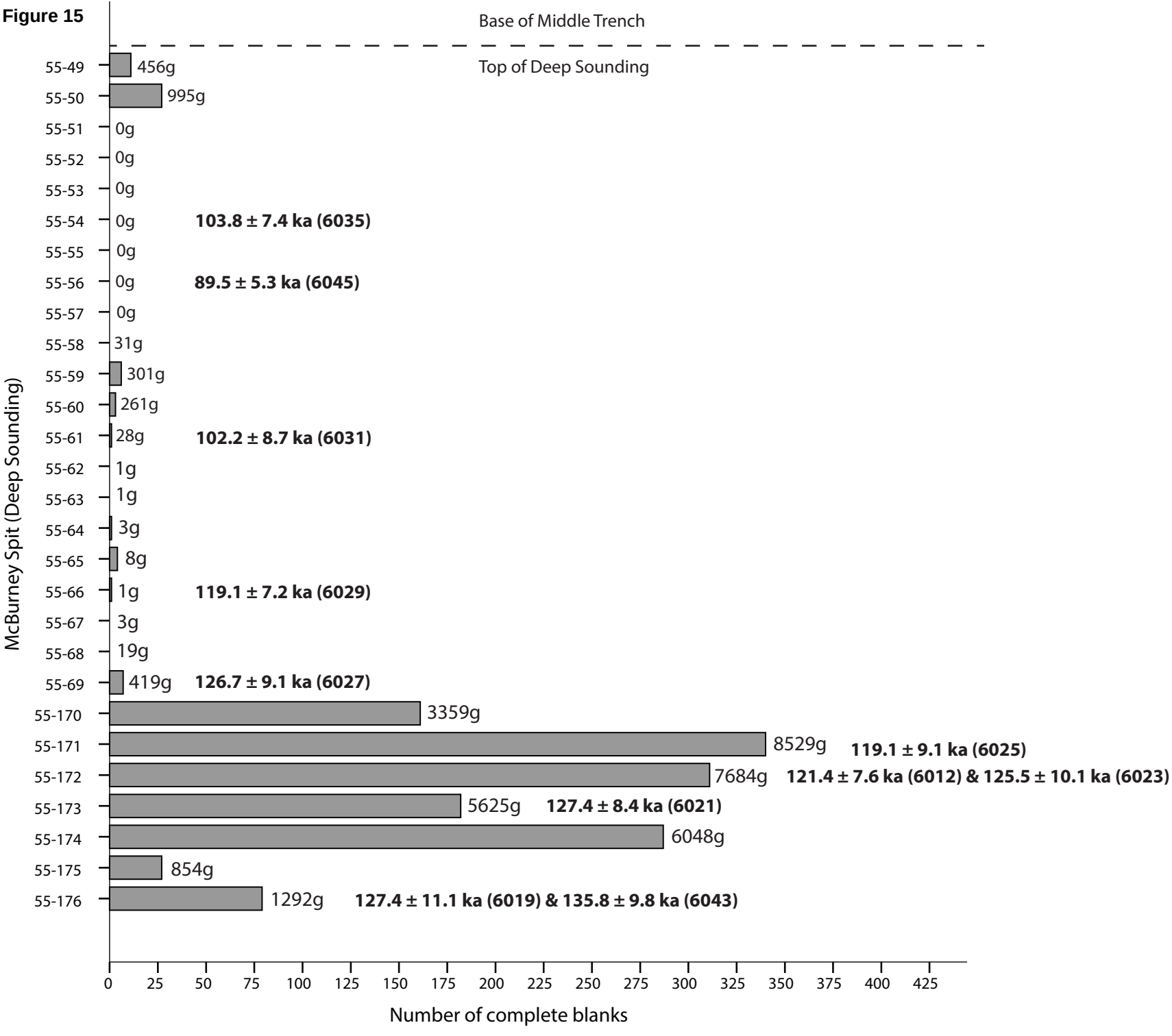
Base of Middle Trench
Top of Deep Sounding
McBurney Spit (Deep Sounding)
55-49 456g
55-50 995g
55-51 0g
55-52 0g
55-53 0g
55-54 0g 103.8 ± 7.4 ka (6035)
55-55 0g
55-56 0g 89.5 ± 5.3 ka (6045)
55-57 0g
55-58 31g
55-59 301g
55-60 261g
55-61 28g 102.2 ± 8.7 ka (6031)
55-62 1g
55-63 1g
55-64 3g
55-65 8g
55-66 1g 119.1 ± 7.2 ka (6029)
55-67 3g
55-68 19g
55-69 419g 126.7 ± 9.1 ka (6027)
55-170 3359g
55-171 8529g 119.1 ± 9.1 ka (6025)
55-172 7684g 121.4 ± 7.6 ka (6012) & 125.5 ± 10.1 ka (6023)
55-173 5625g 127.4 ± 8.4 ka (6021)
55-174 6048g
55-175 854g
55-176 1292g 127.4 ± 11.1 ka (6019) & 135.8 ± 9.8 ka (6043)
0 25 50 75 100 125 150 175 200 225 250 275 300 325 350 375 400 425
Number of complete blanks

Figure 16

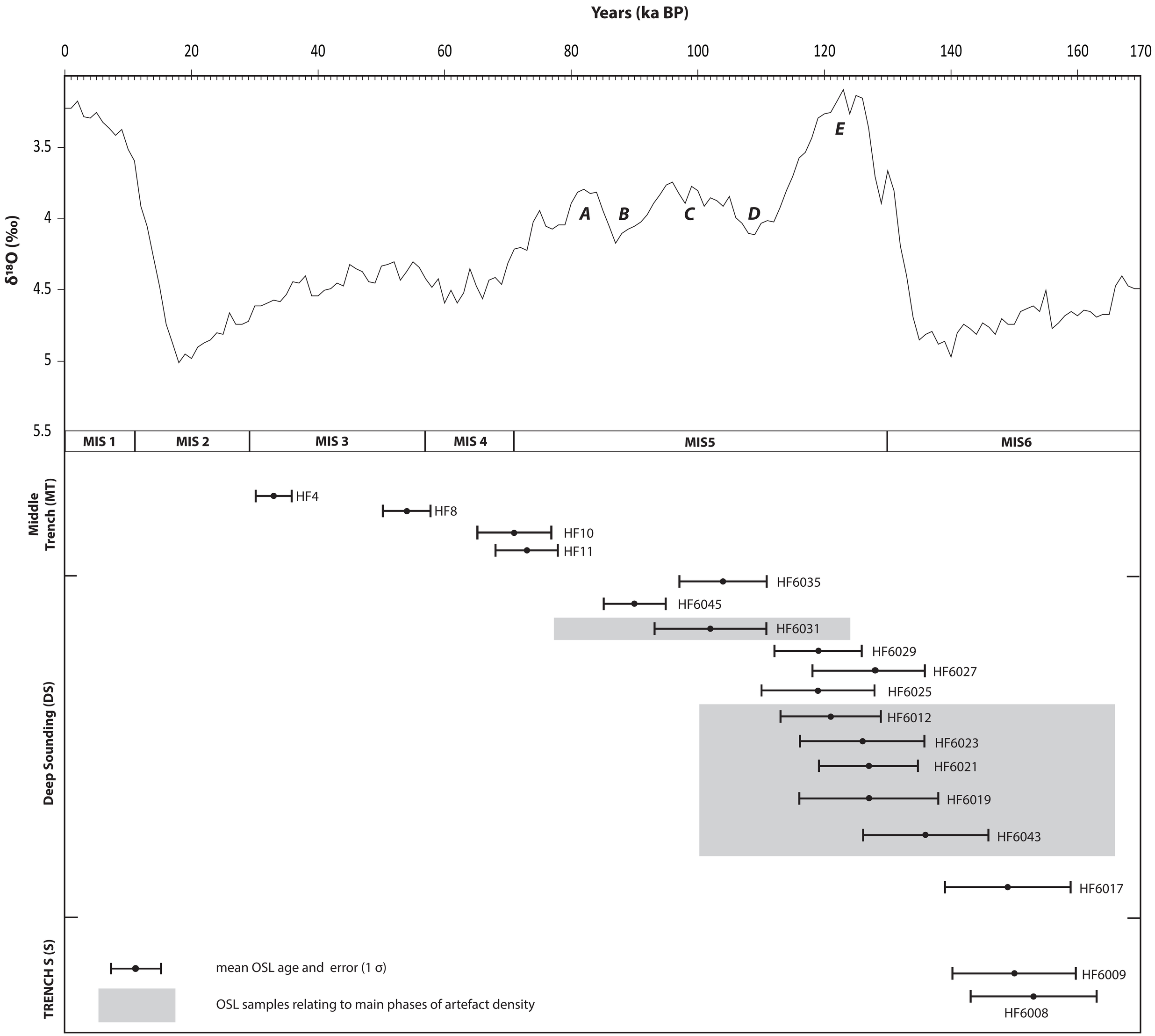
Years (ka BP)
0
20
40
60
80
100
120
140
160
170
δ18O (‰)
3.5
4
4.5
5
5.5
A
B
C
D
E
MIS 1
MIS 2
MIS 3
MIS 4
MIS5
MIS6
Middle Trench (MT)
HF4
HF8
HF10
HF11
Deep Sounding (DS)
HF6035
HF6045
HF6031
HF6029
HF6027
HF6025
HF6012
HF6023
HF6021
HF6019
HF6043
HF6017
TRENCH S (S)
HF6009
HF6008
mean OSL age and error (1 σ)
OSL samples relating to main phases of artefact density